UNIVERSITY OF SUSSEX

THIRD YEAR PROJECT REPORT

Fast methods for building accurate neuron models of individual neurons

Author:
Daniel SASKA

Supervisor:
Prof. Thomas NOWOTNY

A report submitted in fulfillment of the requirements for the degree of BSc (Hons) in Computer Science and Artificial Intelligence

in the

CoNNeCT Group
School of Engineering and Informatics

April 18, 2016

Declaration of Authorship

This report is submitted as part requirement for the degree of BSc (Hons) in Computer Science and Artificial Intelligence at the University of Sussex. It is the product of my own labour except where indicated in the text. The report may be freely copied and distributed provided the source is acknowledged.

Signed:

Date:

UNIVERSITY OF SUSSEX

Abstract

School of Engineering and Informatics

BSc (Hons) in Computer Science and Artificial Intelligence

Fast methods for building accurate neuron models of individual neurons

by Daniel SASKA

The estimation of parameters for models describing single neuron dynamics have been a topic of many research works in the past. With the increasing computational capability, the focus of many researchers exploring the electrophysiological properties of neurons has shifted towards increasingly more automated processes, allowing the construction of more accurate and complex models.

This work investigates the possibility of finding a set of distinctive voltage protocols which are able to isolate the effects of individual parameters of the electrophysiological model of a neuron in order to accelerate the estimation of the correct parameter values using voltage clamp and following this process with parameter estimation on current clamp to further refine the results. Since this method estimates model parameters using data collected from a single neuron, it could be used to find parametrizations for models of individual neurons which could prove useful in future investigation of neuron-to-neuron variance of electrophysiological properties hypothesized in some research works [1].

The estimation method was evaluated using performance on a model of the squid giant axon proposed by Hodgkin and Huxley [2] with 19 parameters and a model of the LP cell in the stomatogastric ganglion of crabs, proposed by Liu et al. [3] with 15 parameters, in which the maximum conductances, reversal potentials and parameters defining calcium concentration were considered unknown. The results of this work have shown that the performance of model parameter estimation on models with interdependent unknown parameters was significantly lower than when the parameters were not as interdependent. It has also been shown that the ability of the protocols to separate the effects of the individual parameters was not uniform over the investigated parameter range and therefore co-evolution of the voltage protocols along with the estimation of the parameters may offer better results. Finally, the application of the method to the stomatogastric ganglion have shown that it is able to make clear distinction between various parametrizations with vastly different parameters but similar spiking rhythms.

Acknowledgements

I would like to thank my supervisor, Professor Thomas Nowotny, for offering me an opportunity to work on a project exploring a very interesting, yet challenging, area of research, and for his guidance which allowed me to gain new knowledge and skills in both the area of computational neuroscience and research procedures in general. Furthermore, I would also like to thank Felix Kern for providing valuable data from his research as well as practical knowledge directly tied to the methods investigated in my work.

Contents

List of Figures

List of Tables

Chapter 1

Introduction

Increasing interest in the properties of the brain, perpetuated by the wide application in medicine and the human desire to understand the underlying causes behind behavioral and physiological processes, requires firm understanding of neurons and neural networks on a multitude of scales. This work focuses on exploring methods helping to enhance the understanding of individual neurons, concretely, it investigates a sequence of estimation techniques forming an universal framework for estimating a correct parametrization of neuron models.

Numerous works with a similar objective have been published in the past several years, succeeding in automating some tasks which have been otherwise done by hand, such as the model parameter estimation from the collected data. However, most methods are unable to estimate the parameters from a single neuron, resorting to use of pharmacological blockers which then requires use of multiple neurons for the data collection. Furthermore, a significant proportion of the methods requires use of a computer cluster for an extensive period of time, which may not be always available. Last major issue with vast majority of the methods is the requirement of user-defined stimuli which are often not extensively justified.

1.1 Methodology overview

This work investigates new approach to estimating parameters for neuron models by first optimizing a set of voltage waveform protocols off-line and then applying them to a neuron in a voltage clamp setting with up to real-time parameter estimation. The results are then carried over to estimation in a current clamp setting which refines the model estimated using a voltage clamp. The background and research related to the investigated methods are discussed in Chapter 2.

1.1.1 Experimentation Environment

To verify the validity and effectiveness of the methods proposed in this work, simulation of well established models is used, and is further discussed in Chapter 4. The reference model, which was used as the objective for the parameter optimization, was executed on a CPU whereas the candidate estimate models (as introduced in the following subsection) were executed on a range of NVIDIA graphics accelerators. The exact specifications of the accelerators are presented where required in the context of establishing the time performance for this parameter estimation method.

1.1.2 Estimation approach

The parameter estimation method consists of two main steps: the off-line voltage protocol waveform generation and the on-line parameter estimation. The on-line parameter estimation then further consists of estimation of the model parameters in the voltage clamp setting followed by an estimation in the current clamp setting. As will be explained in Chapter 5, the waveforms are selected in an attempt for each to highlight the effects of varying one parameter. On the contrary, majority of the methods proposed in the past fail to justify the used stimuli, often resorting to using a number of simple steps or ramps or even use noise as an input.

In the past, it was left up to the neuroscientist to correctly select the voltage protocols, relying on his creativity and correct judgement. The parameter selection introduced in this work is automated by optimization of the information the waveforms offer about the variation of the model parameters.

The voltage protocols are then applied to the observed neuron as well as a population of simulated model estimates in the voltage clamp setting. The population of simulated models is then evolved using a genetic algorithm based on the difference between current injected into the simulated and real neurons, optimizing the ability of the estimated models to reproduce the electrophysiological properties of the real neuron. This process is detailed in Chapter 6 and followed by an estimation in the current clamp setting which is described in Chapter 7. The results of the estimation are then used to show that existence of large variance of parameter values in models with nearly identical spiking pattern as suggested by Golowasch et. al. [1] would be likely discovered, should these variances actually exist in real neurons.

The consecutive combination of voltage and current clamp setting were found to perform particularly well due to the nature of the fitness landscape of each of the settings as is described in upcoming sections.

Chapter 2

Background and Related Work

2.1 Electrophysiological properties of neurons

The formulation of the ionic current model of a neuron as it is widely known today has started with results published by Overton in 1902, who has noticed that the frog muscle became inexcitable when immersed in solutions of less than 10% of the usual sodium concentration [4] which lead to the first formulation of the ionic hypothesis. This formulation was later regarded as incomplete and updated by Hodgkin and Katz in 1949 [4] along with experimental analysis of the new hypothesis. The updated ionic hypothesis explains the formation of action potentials through a description of electrophysiological properties of the neuron membrane as described below.

At rest, the membrane is more permeable to potassium than sodium, allowing easier diffusion of potassium through the membrane. Conversely, the permeability to sodium ions of the resting membrane was found to be very low and compensated for by active sodium pumps which expend energy to move the sodium ions against the diffusion gradient, maintaining the intracellular sodium concentration at about 10% of that of the extracellular solution.

The resting potential of the cell can be calculated using the Goldman-Hodgkin-Katz equation:

$$V = \frac{RT}{F} ln\left(\frac{p_K[K^+]_{out} + p_{Na}[Na^+]_{out} + p_{Cl}[Cl^-]_{in}}{p_K[K^+]_{in} + p_{Na}[Na^+]_{in} + p_{Cl}[Cl^-]_{out}}\right) \tag{2.1}$$

where V is the membrane potential in volts, p_{ion} is the membrane permeability for the ion indicated by subscript in $\mathrm{m\,s^{-1}}$, $[ion]_{in}$ and $[ion]_{out}$ are the intracellular and extracellular concentrations for the indicated ion in $\mathrm{mol\,m^{-3}}$, respectively, and R, T and F are the ideal gas constant in $\mathrm{J\,mol^{-1}\,K^{-1}}$, temperature in kelvin and Faraday constant in $\mathrm{C\,mol^{-1}}$, respectively.

The permeability to sodium ions, however, increases if the membrane is sufficiently depolarized by direct current injection or through other neuron processes, further depolarizing the membrane and forming the rising phase of the action potential. As a result of this process, the voltage potential of the inside of the cell briefly becomes positive with respect to the outside, causing outflow of the potassium ions through the outward potassium channels with the (now) increased permeability. With the sodium permeability decreasing over time (illustrated in Fig. 2.1), the outflow of the positively charged potassium becomes significantly greater than influx of the sodium, resulting in rapid repolarization, reverting the membrane to the previous resting potential [5].

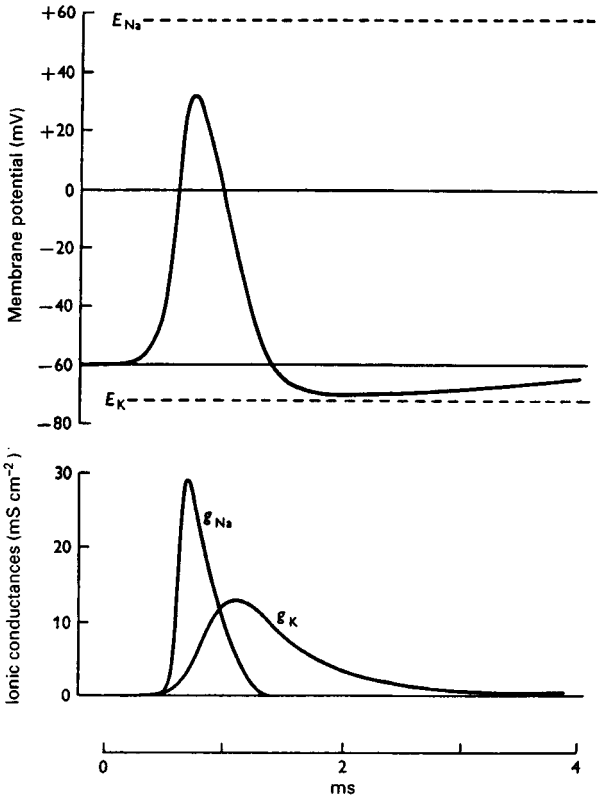

FIGURE 2.1: **Relation of the conductances to the rising and falling phase of the action potential.**
Upper plot displays the membrane potential and lower plot shows the permeability of the membrane to the sodium and potassium ions. Taken from *The physiology of excitable cells* [6], redrawn from Hodgkin and Huxley, 1952 [2].

2.2 Hodgkin-Huxley model

The first universal and widely accepted approach to modelling of the electrophysiological properties of neurons has been formulated by Hodgkin and Huxley in 1952 [2], building on observations from their preceding research focusing on the squid giant axon. Hodgkin and Huxley have suggested that the electrical current can be carried over the cell membrane either by ionic current or by charging up the membrane capacity. The ionic current represents the current resulting from movement of charged particles over the membrane through ionic channels and pumps. The electrophysiological properties of a squid giant axon have been observed to rise up primarily from the dynamics of sodium and potassium ion current (I_{Na}, I_K), secondly then from a flow of chloride and other ions which were, due to their low significance to the dynamics of the overall system, in the model represented as a single ionic current (I_{leak}) which is commonly also referred to as leakage current. Naturally, for cells with more complex dynamics and as the understanding of neurons advances, researchers are able to distinguish more ion channels and build more complex models, but even so, adding the leakage current to the models has become common practice in an attempt to account for some of the neuron properties which cannot yet be accurately described.

Based on Hodgkin and Huxley's research, it is now widely accepted that the current across the neuron membrane can be described as

$$I = C\frac{dV}{dt} + \sum I_i, \tag{2.2}$$

where I is the total membrane current, I_i is the current resulting from the flow of ions through channel i, C is the membrane capacitance, V is the voltage potential difference across the neuron membrane and t is time.

The individual ionic currents are then modelled based on the ionic conductances and equilibrium potentials. For the squid giant axon then

$$\begin{aligned} I_{Na} &= g_{Na}(V - E_{Na}) \\ I_K &= g_K(V - E_K) \\ I_{leak} &= g_{leak}(V - E_{leak}) \end{aligned} \tag{2.3}$$

where subscripted I, g and E are ionic current, ionic conductance and equilibrium potential, respectively, for the ionic channel indicated by the subscript. Equation 2.3 can be similarly applied to models for different neuron types as noted later in this chapter. The individual conductances are then described as

$$\begin{aligned} g_K &= n^4\overline{g}_K \\ \frac{dn}{dt} &= \alpha_n(1-n) - \beta_n n \end{aligned} \tag{2.4}$$

$$\begin{aligned} g_{Na} &= m^3 h\overline{g}_{Na} \\ \frac{dm}{dt} &= \alpha_m(1-m) - \beta_m m \\ \frac{dh}{dt} &= \alpha_h(1-h) - \beta_h h \end{aligned} \tag{2.5}$$

where $\overline{g}_K$ and $\overline{g}_{Na}$ are the maximum conductances per unit area for given

Parameter	$\overline{g}_{Na}$	E_{Na}	$m_{a,off}$	$m_{a,slope}$	$m_{b,off}$	$m_{b,slope}$	$h_{a,off}$	$h_{a,slope}$	$h_{b,off}$	$h_{b,slope}$
True model	120.00	55.00	3.50	0.1000	60.00	18.00	3.00	20.00	3.00	0.1000

Parameter	$\overline{g}_{K}$	E_{K}	$n_{a,off}$	$n_{a,slope}$	$n_{b,off}$	$n_{b,slope}$	g_l	E_l	C_{mem}
True model	36.00	-72.00	0.500	0.01000	60.00	80.00	0.30	-50.00	1.0

TABLE 2.1: **Parametrization of the squid giant axon model.**

channels, n, m and h are dimension-less variables in interval $[0, 1]$ and t is time. α and β for the n, m and h variables are then functions of V described as

$$\begin{aligned} \alpha_n &= \frac{-n_{a,off} - n_{a,slope}V}{exp(-10.0n_{a,off} - 10.0n_{a,slope}V) - 1.0} \\ \beta_n &= 0.125exp(\frac{-V - n_{b,off}}{n_{b,slope}}) \end{aligned} \tag{2.6}$$

$$\begin{aligned} \alpha_m &= \frac{m_{a,off} + m_{a,slope}V}{1.0 - exp(-m_{a,off} - m_{a,slope}V}) \\ \beta_m &= 4.0exp(\frac{-V - m_{b,off}}{m_{b,slope}}) \end{aligned} \tag{2.7}$$

$$\begin{aligned} \alpha_h &= 0.07exp(-\frac{V}{h_{a,slope}} - h_{a,off}) \\ \beta_h &= \frac{1.0}{exp(-h_{b,off} - h_{b,slope}V) + 1.0} \end{aligned} \tag{2.8}$$

where constants are obtained by fitting the collected data and presented in Table 2.1. Note that g_{leak} is a voltage-independent constant.

2.3 Pharmacological channel blockers

Pharmacological blockers have been an essential tool in the investigation of the electro-physiological properties of neurons until early 21st century because extensive computational power was not available, making estimation of complex models impossible. Pharmacological blockers can greatly simplify the task since it is possible to partially or completely block certain ion channels, effectively reducing the complexity of the estimated model. Multiple of such models can then be composed into the complete model which makes blockers an attractive tool even now.

2.3.1 Commonly used pharmacological blockers

Tetrodotoxin (TTX), poison isolated from the Japanese puffer fish, was found to selectively inhibit the sodium-carrying mechanisms of neurons without affecting the potassium-carrying system [7]. Tetrodotoxin is reversible, however the extent depends on how well the procedure is executed [8][9] and the reversibility was found to be improved when high concentration of calcium was applied along with the toxin [10]. Even so, relying on the chance (even if higher with skill) of executing the procedure well, for the purpose of model estimation, may be problematic because the measurements collected after the reversal may be still affected by small amounts of toxin remaining after the through, yet incomplete, removal of TTX. Rather

than relying on washing away the pharmacological blockers when possible (such as in the case of TTX), it has become common to use multiple cells with different (sets of) blockers applied.

Tetraethyamonium (TEA) is a synthetically created potassium-selective ion channel blocker usually used together with TTX in investigating the dynamics of sodium and potassium ion channels [11]. The effects are reversible, however the situation is similar to TTX. Removal of potassium from the extracellular solution has been shown to cause the TEA blockade to irreversibly reduce the potassium current even after the blocker is washed away. In some cells, TEA was shown to block more than one (potassium) current such as in the stomatogastric ganglion neurons where it simultaneously blocks the calcium-dependent outward current and the delayed rectifier current [12] described in the section 2.4.

Other pharmacological blockers are used for experimentation on more complex cells, such as aforementioned stomatogastric ganglion neurons. Examples include cadmium [12], 4-aminopyridine (4AP) [12] or charybdotoxin (CTX) [13]. Some methods also include the removal or replacement of a substance in the extracellular solution in order to deprive the cell of means to facilitate some of its function such as a replacement of calcium to block the calcium-dependent outward current [14].

2.3.2 Problems with application

For the reversible blockers, it often takes time to wash away the toxins to revert the cell back into its previous state which could otherwise be used for data-collection, not to mention the issues of incomplete removal of the blockers.

The variance in the types of ion channels also pose problem to the application of pharmacological blockers. Different ion channel types may react to the same blocker differently, the puffer fish itself poses prime example of this phenomenon, having evolved sodium ion channels which are particularly resistant to TTX [15].

2.4 Stomatogastric ganglion

Neurons which have complex electrophysiological dynamics, consisting of a multitude of ion channels, have been recognized as the type of neurons that participates most in the generation of complex behaviours [16]. This motivated many scientists to examine electrophysiological properties of neurons with complex dynamics such as the stomatogastric ganglion (STG) neurons of crab and lobster which were shown to vary their electrophysiological properties over their lifetime [17] and are responsible for motor functions of stomach muscles in those invertebrates [18]. It is only natural that with more complex electrophysiological dynamics of the observed cell, neuroscientists also have to employ new, more advanced, techniques in order to model the behaviour accurately.

The stomatogastric ganglion cells in lobster and crab have been of particular research interest mainly because the ganglion comprises a rather low number of cells. With the aim to sufficiently characterize the nature all of

the neurons and interconnections, neuroscientists hoped to advance the understanding of how the control of stomach muscles is initiated in these animals

2.4.1 Electrophysiological properties of a stomatogastric ganglion neuron

A number of ionic current mechanisms have been identified by many works. These include

- **Sodium Currents** - Two voltage-activated inward sodium currents are identified in the STG. First, as discussed by Hodgkin and Huxley [2], fast voltage-activated transient current which drives the rising phase of the action potential [19]. Second is the low-threshold persistent current which is one of the mechanisms for plateau activation and maintenance [19](See below). It has been suggested, however, that the persistent sodium current could originate from sub-threshold activation of the transient current channel type, rather than from channels of a distinct type [20].

- **Calcium-Dependent Outward Current** - A fast activating and inactivating calcium-dependent outward current which was found to contribute to the potassium outward current and thus lead to a shorter falling phase and higher hyper-polarization after an action potential [12]. Furthermore, this outward current has been shown to play a role in plateau termination [21].

- **A-Current** - A transient outward potassium channel with fast activation and moderately slow inactivation [14]. The A-Current have been shown to delay the spike and burst activation and therefore plays a role in the regulation of the cycle frequency, although the effects of the current differ in each neuron. Pharmacological blockage of the current using 4-AP resulted in increased cycle frequency of the spike bursts and increased spike activity as well as amplitude during the bursts in some neurons [22].

- **Delayed Rectifier Current** - An outward rectifier current which facilitates the falling phase of the action potential [2][14].

- **Pacemaker Current** - An inward rectifier hyper-polarization activated current with slow activation, often also called "sag" current [14][21]. The sag current was shown to be modulated by an extracellular concentration of some substances such as serotonin, which has shown to decrease the activation time of this current and thus increase its excitability [21].

- **Calcium-activated non-selective cation current** - A slow inward non-selective current which participates in the maintenance of the plateau potential [23].

- **Calcium Channels** - Intracellular calcium plays a major role in many processes of the neuron thorough activation of a number of the currents mentioned above [23]. Many models have included fast and slow inward calcium current components, however the details of these

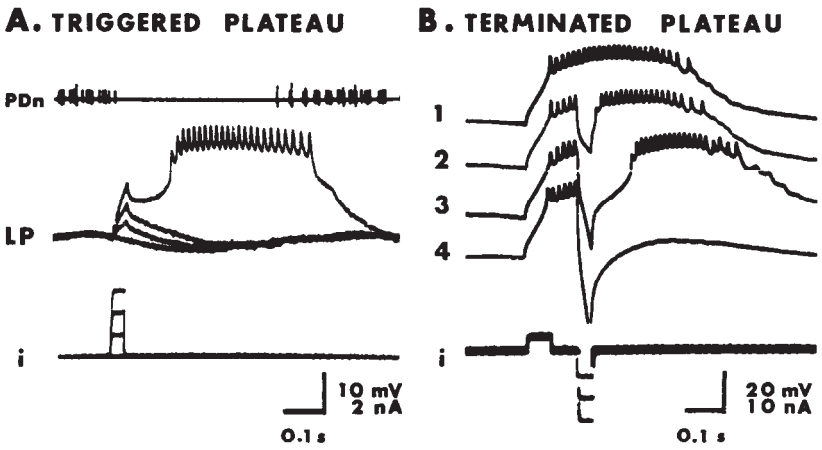

FIGURE 2.2: **Illustration of plateau activation and termination with current stimulus published by Hartline et al. [24].**

components differ between models [3][17]. The calcium channels have shown to be activated or suppressed by extracellular agents which causes indirect modulation of the calcium dependent currents, altering the behaviour of the cell [23].

Not every current was found in all neurons of the stomatogastric ganglion. The currents included in the model used in this work are noted in Section 2.4.2.

Plateau properties

A plateau potential is defined as a self-sustained depolarized state, usually accompanied by an intense burst of spikes. The opposite is also usually true when the neuron is not in the plateau state: the neuron is below the threshold potential and does not produce action potentials, or at much lower rate than when in the plateau state. The plateau has been shown to be initiated by brief depolarizing current stimulus and terminated by hyperpolarizing current stimulus (See Fig. 2.2)

Adaptation properties

Neurons display the ability to *adapt* to continuous stimuli and their firing frequency decays over time. The rate of decay seems to decrease exponentially over time when the cell is stimulated with constant current but seems to be relatively current-independent for the studied range [25].

Delaying properties

Some neurons in the stomatogastric ganglion display the property of delaying the response to stimulus [26].

Post-inhibitory Rebound

Some STG neurons have been observed to rapidly return to the plateau potential with temporarily increased spiking rate after a hyper-polarization by injection of negative current or synaptic inhibition [25].

2.4.2 Neuron model definition

For purposes of this work, the stomatogastric ganglion neuron model used is based on the conductance-based model introduced by Liu et. al. [3] which follows the Hodgkin and Huxley format. The membrane current is expressed using Eq. 2.2 and the individual ionic channels follow equations based on Eq. 2.3 with reversal potentials specified in Table 2.2. The included currents are the fast sodium current (I_{Na}), the transient and slow calcium current (I_{CaT}, I_{CaS}), the A-Current (I_A), the calcium-dependent potassium current (I_{KCa}) and delayed potassium rectifier current (I_{Kd}).

The ionic conductances, g_i of the individual ion channels then follow

$$\begin{aligned} g_i &= \overline{g}_i m^p h \\ \frac{dm}{dt} &= (m_\infty - m)/\tau_\infty \\ \frac{dh}{dt} &= (h_\infty - h)/\tau_\infty \end{aligned} \tag{2.9}$$

according to Eq 2.6, with m_∞, h_∞, τ_∞ and τ_∞ terms and coefficient p specified in Table 2.2, h term is omitted for channels missing associated terms in the table.

The calcium concentration, $[Ca]$, follows the equation modified according to Golowasch et. al. [1]:

$$\frac{d[Ca]}{dt} = -(Ca_f \times (I_{CaT} + I_{CaS}) - [Ca] + Ca_0)/Ca_t \tag{2.10}$$

, where $Ca_f = 14.96\mu\text{M}\,\text{nA}^{-1}$, $Ca_0 = 0.05\mu\text{M}$ and $Ca_t = 200\text{ms}$.

	p	E	m_∞	h_∞	τ_m	τ_h
I_{Na}	3	50	$\frac{1}{1+exp\left(\frac{V+25.5}{-5.29}\right)}$	$\frac{1}{1+exp\left(\frac{V+48.9}{5.18}\right)}$	$1.32 - \frac{1.26}{1+exp\left(\frac{V+120}{-25.0}\right)}$	$\frac{0.67}{1+exp\left(\frac{V+62.9}{-10.0}\right)} * \left(1.5 + \frac{1}{1+exp\left(\frac{V+34.9}{3.6}\right)}\right)$
I_{CaT}	3		$\frac{1}{1+exp\left(\frac{V+27.1}{-7.2}\right)}$	$\frac{1}{1+exp\left(\frac{V+32.1}{5.5}\right)}$	$21.7 - \frac{21.2}{1+exp\left(\frac{V+68.1}{-20.5}\right)}$	$105 - \frac{89.8}{1+exp\left(\frac{V+55}{-16.9}\right)}$
I_{CaS}	3		$\frac{1}{1+exp\left(\frac{V+33}{-8.1}\right)}$	$\frac{1}{1+exp\left(\frac{V+60}{6.2}\right)}$	$1.4 + \frac{7}{exp\left(\frac{V+27}{10}\right)+exp\left(\frac{V+70}{-13}\right)}$	$60 + \frac{150}{exp\left(\frac{V+55}{9}\right)+exp\left(\frac{V+65}{-16}\right)}$
I_A	3	-80	$\frac{1}{1+exp\left(\frac{V+27.2}{-8.7}\right)}$	$\frac{1}{1+exp\left(\frac{V+56.9}{4.9}\right)}$	$11.6 - \frac{10.4}{1+exp\left(\frac{V+32.9}{-15.2}\right)}$	$38.6 - \frac{29.2}{1+exp\left(\frac{V+38.9}{-26.5}\right)}$
I_{KCa}	4	-80	$\left(\frac{[Ca]}{[Ca]+3}\right)\left(\frac{1}{1+exp\left(\frac{V+28.3}{-12.6}\right)}\right)$		$90.3 - \frac{75.1}{1+exp\left(\frac{V+46}{-22.7}\right)}$	
I_{Kd}	4	-20	$\frac{1}{1+exp\left(\frac{V+70}{-6}\right)}$		$7.2 - \frac{6.4}{1+exp\left(\frac{V+28.3}{-19.2}\right)}$	

TABLE 2.2: Table describing the dynamics of the STG neuron as presented by Liu et al. [3]

2.5 Problem of using multiple neurons

It is common practice in neuroscience, and science in general, to use multiple measurements to avoid random error and to uncover any unexpected

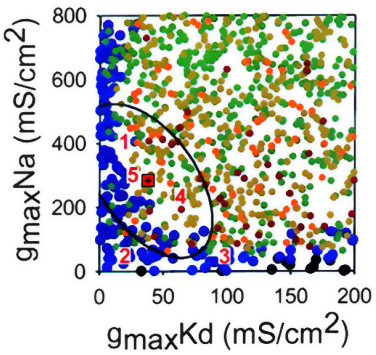

FIGURE 2.3: **Categorization of neurons by the number of spikes per burst.** 0: black, 1: blue, 2: green, 3: olive, 4: orange, 5: burgundy as presented by Golowasch et al. [1].

circumstances or deviations that would otherwise remain hidden to a scientist if only one trial was to be done. The collected data is usually averaged under the assumption that the resulting representation will better illustrate the overall data that was observed and thus will be a more robust solution than any single observation on its own.

This assumption was theoretically examined using the stomatogastric ganglion neuron model parametrization (as mentioned in the section 2.4.2) as an example by Golowasch et al. [1]. A number of models parametrized with a range of values for the conductances of the individual ion channels were observed with the aim to categorize them based on their endogenous spiking patterns into the groups of (zero), one, two, three, four and five-bursters based on the number of spikes exhibited per one burst.

The results, shown in Figure 2.3, have indicated that the one-spike bursters (blue in the figure) lie in a "L"-like shape where each of the data samples has at least one of the two conductances (sodium and/or potassium) considerably low. When the parameters of one-spike bursters have been averaged, the resulting model not only did not lie in the space which was rather rare for one-spike bursters, but also itself was a three-spike burster. This issue is going to affect various models to different extent, mainly depending on the stability of the model, i.e. to what extent do the properties of the model change when parameters are altered, as well on the convexity of the parameter regions for which the models exhibit very similar behaviour (consider the unconvex "L" shape for one-spike bursters in this example).

The issues affecting the averaging method would also affect methods using chemical blockers and observing channels separately in different neuron preparations which includes significant portion of the parameter estimation approaches in the past.

2.6 Automated methods

With the increasingly sufficient computational power in the early 2000s, automated methods for parameter estimation started to become common trend in publications in the field of computational neuroscience. This eliminated some problems of the previous methods, namely the need for extensive human involvement not only in the data collection but also the parameter estimation.

A number of the publications indicate that genetic algorithms are suitable for global search of the parameter space but can be improved on by using a localized search strategy afterwards [27][28][29]. However, methods using different approaches to estimation have been proposed as well, including simulated annealing [28], differential evolution [28] and swarm optimization [30][31].

The divide between experimentalists and theorists in the area of neuroscience proves to be an increasing problem as the scientists who focus on experimentation and have great skill in the experimental methods often lack the extensive knowledge needed to use or even implement the state-of-art methods developed by computational neuroscientists. With the increasing involvement of computation in (not only) the field of neuroscience, this is becoming a problem preventing fast paradigm shift in these areas since experimentalists prefer to use manual approaches to tasks which could otherwise be automated with computation. This became a motivation for theorists to implement user-friendly environments for their software solutions such as the NEUROFIT method [32].

2.7 GPU-Accelerated programming

With the increasing difference in the computational capability of CPU and GPU, the graphics processors are being used more and more in applications where parallelization of the computational task is possible. These areas include primarily computer science and physics but neuroscience can benefit from the parallel computation as well. The ability to simulate a large number of neurons is useful in simulations of neural networks but also in parameter estimation and other areas.

GPU-accelerated programming can in some cases eliminate the need to have access to large computer clusters and instead run on a single machine with comparable performance as illustrated in a number of parameter estimation methods [30][33][34], proving the potential of parallel computation to become a new standard in parameter estimation methods.

2.8 GeNN Framework

GeNN (GPU-enhanced Neuronal Networks) framework facilitates the functionality of simulating neural networks consisting of a large number of user-defined neurons using parallel processing power of modern graphics accelerators supporting NVIDIA CUDA architecture. As mentioned in the previous section, this approach can be applied to parameter estimation methods as well and is used to facilitate the processing of neuron populations in this work.

2.9 Genetic Algorithms

Genetic Algorithms are a family of optimization strategies based on the theory of evolution. Taking inspiration in biology, genetic algorithms define a subset of potential solutions to a problem as a population of individuals

defined by chromosomes where genes represent the parameters of the solutions. Since the full set of potential solutions is in most cases too large (or even infinite) to be exhaustively searched, the population is in comparison small in size, with random initialization of genes to cover most of the search space. The algorithm then iterates the population through copying, mutating and crossing-over the genes with the aim to preserve the individuals in areas with higher fitness, gradually decrease the subspace searched, transferring from global search to localized search in several *areas of interest*.

The approach to selecting which individuals should *survive* and be copied to the following generation is of major debate of the scientist community mainly because different problems have been shown to be best solved with different approaches. Distinctive factor of genetic algorithms is selecting (usually) two individuals from the population and combining their genes to create an offspring. Other approaches then suggest copying selected individuals over other ones and altering their genes. The selection of the individuals itself can be done in multiple ways, always in the best attempt to increase the fitness of the individuals. The most common selection schemes include [35]:

- Tournament selection - A subset of individuals of the population is chosen, individuals in this subset are compared against each other and the best one is preserved. This process is then repeated.
- Truncation selection - A subset of presently fittest individuals is retained and replaces the less fit individuals.
- Linear ranking selection - Then individuals are sorted and assigned ranks from 1 to N with N being the fittest. The individuals are then selected with probability proportional to the rank divided by the sum of all rank values in the population.
- Exponential ranking selection - Same as above but the selection is done according to ranks to the power $0.0 < p < 1.0$ where p is constant across the ranks.
- Proportional selection - Similar to linear ranking selection but the probability of selection depends on fitness of each individual rather than its rank.

It is also common to keep one or more individuals in the *elitist* population to prevent the most likely solutions from being lost.

Termination of the algorithm is also rather rich in options, based on what is applicable to a given problem. The main approaches include:

- Reaching a solution with satisfactory fitness
- Reaching a fixed number of generations
- Allocated computation time is depleted
- Successive iterations no longer produce individuals with improved fitnesses or the improvement is below threshold

Due to the large amount of options, this optimization method as often been avoided and labelled as *black art*. However, when used with caution, genetic algorithm can become optimization technique which does not require careful initialization, requires no prior knowledge about the system and is able to avoid local minima which can be problem for other approaches such as gradient descent.

2.10 Numerical methods for solving differential equations

The method of solving the differential equations of the electrophysiological variables plays a role in how well the model will approximate the real neuron. With a (extremely) poorly selected method, the model may become unstable under some inputs or even in situations to which the normal neuron would be commonly subjected. The two common approaches are the Euler method and the family of Runge–Kutta methods. The Euler method is simpler and features constant time step, Runge–Kutta methods then allow variable time step.

The size of the time step affects how well the solution will approximate the differential equation, in theory smaller time steps are always better as they better represent the gradient at the current time defined by the derivative.

In practice, however this is not necessarily the case since the floating point number representation on modern architectures always comes with rounding errors (depending on the architecture and size of the number representation). The smaller time steps require a higher number of iterations over a specific period of time resulting in proportionally more floating point number operations being executed which then in turn increases the error. The Runge–Kutta methods can deal with this by varying the time step as necessary to minimize the error of approximating the gradient while being able to decrease the step count when the error is small. These methods are, however, less suitable for parallel acceleration on the GPU as the CUDA architecture benefits from same set of instructions being executed on all threads but it would be incorrect to assume that the error of the approximation is small (or large) for all of the simulated neurons at the same time as the model may vary or spike at different times.

2.11 Pre-generated waveforms as means to achieve real-time parameter estimation performance

The original work which inspired this project is the unpublished work on parameter estimation using pre-generated voltage waveform protocols in order to accelerate voltage clamp performance done by Thomas Nowotny [36].

The proposed approach consists of generating waveform protocols and subsequently applying them to the neuron in the voltage clamp setting. It is suggested to use genetic algorithm optimizing the fitness function defined in Eq. 5.1 for a fixed number of epochs and in this way generate a protocol for each of the observed parameters. It has been assumed that the efficiency of the waveforms in separating the parameter effects is uniform

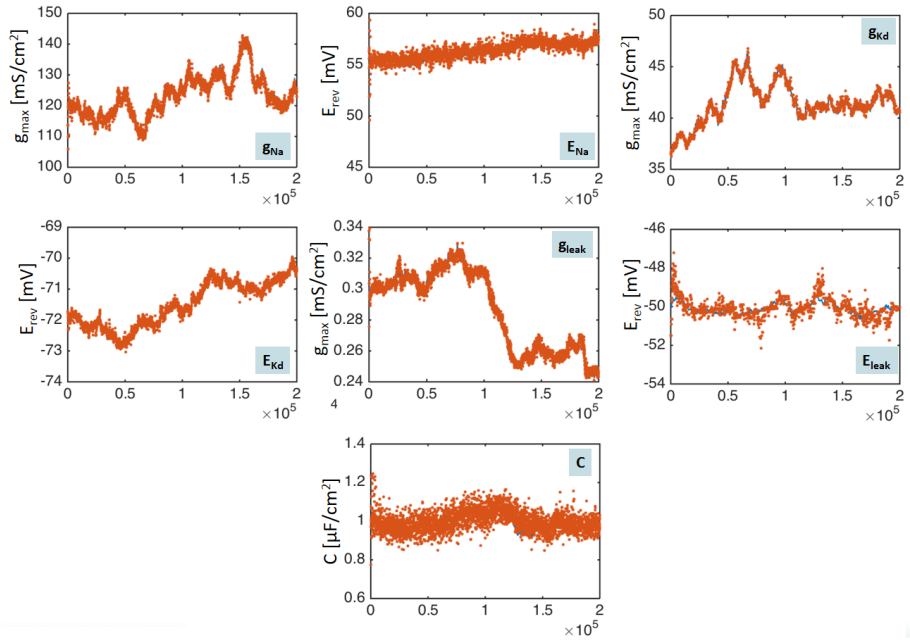

FIGURE 2.4: **Following the parameters of a drifting cell using the parameter estimation strategy with population size of 446805 [36].**

across the investigated parameter range and therefore the prototype uses the true model as reference to estimate the optimal waveforms even though the true model is not known yet at that point in the estimation process.

These waveforms are then applied to a real neuron as well as a population of potential neuron models on a voltage clamp on which expends Chapter 6 again using genetic algorithm. Here the method is altering between the parameters but the next stimulus is used only if the parameter is improvement beyond certain threshold in the past few generations.

This approach was successfully applied to the squid giant axon model, able to converge with 7 unknown parameters on the voltage clamp but it was not compared to the alternative of a simple random stimulus. The ability of the model to produce spiking behaviour typical to that of a real neuron was not tested.

For this simple example, this approach was shown to be able to track parameters of a drifting cell at they change over time as shown in Figure 2.4.

Chapter 3

Ethical Considerations

This research project only uses widely available hardware and software with no undisclosed parts, allowing easy reproduction of results as well as use in further research and applications. Source code and exhaustive description of platform used (both software and hardware-wise) is provided along with this document and is referenced in appropriate sections.

This document includes results of all trials with no hand selection done to potentially alter the results of the experiments and thus lower the credibility of this research work. The results in the main body of this document may, however, be selected from the collected data for the purposes of discussion. The data which is not suitable for discussion will be presented in exhaustive lists of figures in appropriately referenced appendix where possible.

This research project explores a field of theoretical computer science which is well within domain of author's knowledge and competence as it directly relates to his area of education. The background reading that has been done in relation to this project has been summarized in Chapter 2.

This work does not include practical trials of the proposed methods. However, to increase credibility of the experiments done, Felix Kern provided voltage clamp recordings so realistic noise levels can be incorporated into the simulated neuron models. This data was not collected exclusively for this work, it has been pre-recorded for purposes of Felix's own work and then shared upon request. The provided data was collected, shared and used in compliance to BSC Code of Conduct and this section. The data was collected during experiment done on snails which are not protected by Animals (Scientific Procedures) Act , higher animals or human subjects were not be used for purposes of this work and therefore ethical clearance is not needed. By re-purposing data collected for other work, the author attempts to minimize the number of animals used for this project.

All work produced by third-party is well attributed with no attempt of deceit, either through references or the Related Work chapter which contains referenced research carried by other researchers in the past as well as the original work by Thomas Nowotny used as basis for this project.

Finally, all work directly or indirectly related to this research project is carried out in compliance with the law of the United Kingdom.

Chapter 4

Model simulation

This section introduces the channel models and simulation environment for testing the methods proposed in the following chapters. As mentioned in the section 2.10, it is important to correctly select a method for numerical integration of the differential equation to minimize the error caused by the numerical approximation while maintaining computational performance and avoiding error caused by floating point operations.

4.1 Channel Models

Two channel models are used to evaluate the parameter estimation performance of the proposed framework. First, the Hodgkin-Huxley model for the squid giant axon for its simplicity which allows close to full parametrization of the model with 19 parameters. The estimated parameters include the membrane capacitance, maximum conductances, reversal potentials and constants defining the slope and offset of the channel-defining sigmoid functions. The true parameters along with the investigated range is indicated in Table 4.1.

Estimation of correct parametrization of such a model is comparable to state-of-the-art methods which are able to obtain sufficient results on models with 12-16 parameters. Furthermore, attempting to estimate all parameters of the model will allow evaluation of the performance on parameters which are affecting the model in very different ways (e.g. consider conductances vs variables of the sigmoid defining the channel dynamics).

The second channel model used is the stomatogastric ganglion neuron model proposed by Liu et al. [3] and modified by Golowasch et al. [1]. The main objective of using this model is to show whether or not the parameter estimation framework is able to reconstruct the parameter sets published

Parameter	$\overline{g}_{Na}$	E_{Na}	$m_{a,off}$	$m_{a,slope}$	$m_{b,off}$	$m_{b,slope}$	$h_{a,off}$	$h_{a,slope}$	$h_{b,off}$	$h_{b,slope}$
Minimum	1.0	0.0	2.5	0.06	50.0	12.0	2.0	12.0	2.0	0.06
Maximum	500.0	100.0	4.50	0.14	70.0	24.0	4.0	28.0	4.0	0.14
True model	120.0	55.0	3.5	0.1	60.0	18.0	3.0	20.0	3.0	0.1

Parameter	$\overline{g}_{K}$	E_{K}	$n_{a,off}$	$n_{a,slope}$	$n_{b,off}$	$n_{b,slope}$	g_l	E_l	C_{mem}
Minimum	1.0	-100.0	-0.5	0.006	50.0	48.0	0.1	-100.0	0.1
Maximum	500.0	-0.0	1.5	0.014	70.0	112.0	500.0	0.0	10.0
True model	36.0	-72.0	0.5	0.01	60.0	80.0	0.3	-50.0	1.0

TABLE 4.1: **Parametrization of the squid giant axon model with the investigated range.**

Parameter	C	g_{Na}	g_{CaT}	g_A	g_{KCa}	g_{Kd}	g_{leak}	E_{Na}	E_A	E_{KCa}
Minimum	0.1	0.0	0.00	0.0	0.0	0.0	0.0	0.0	-100.0	-100.0
Maximum	10.0	800.0	5.00	75.0	300.0	200.0	1.0	100.0	0.0	0.0

Parameter	E_{Kd}	E_{leak}	Ca_f	Ca_0	Ca_t
Minimum	-100	-100.0	14.0	0.010	20.0
Maximum	0.0	0.0	16.0	0.100	250.0

TABLE 4.2: **Parametrization of the stomatogastric ganglion model with the investigated range.**

by Golowasch et al. and thus show if the proposed framework can avoid the issue of averaging [1]. The maximum conductances, reversal potentials and variables defining the calcium concentration are considered unknown along with the ion channel conductances to increase the complexity of the estimation problem in this setting to be comparable to the problems solved by state-of-the-art methods. Furthermore, assuming the variables defining the activation and deactivation dynamics to be constant may be realistic even in real world applications since assuming that the internal dynamics of the ion channels do not vary from neuron to neuron is reasonable. Table 4.2 shows the parameter ranges used during the estimation, the reference models are specified in appropriate sections where necessary.

4.2 Model simulation

The *real neuron* model is simulated on CPU in order to supply data which would otherwise be obtained from the electrode reading on a real neuron. A population of simulated neuron models which aim to replicate the behaviour of the real neuron (this process is detailed in the following chapters) run on the GPU in parallel. Since the simulated neurons are integrated in parallel on the GPU, it is necessary to use a method which follows the same execution on all threads i.e. integration method with constant time step. The following section investigates the best possible application of Euler method with the objective to minimize the integration error.

Gaussian noise was added to the reading from the *real neuron* in both clamp modes, with standard deviation of 0.23nA for the current reading and 0.10mV for the voltage reading, based on experimental data[1].

4.2.1 Methodology

Since the Euler method does not consider the possibility of decreasing the step count when the numerical approximation error is low, it is necessary to show that the floating point operation error does not pose significant problem to the quality of the approximation. Considering a current clamp setting, the neuron models are simulated on the GPU with varying time step length. The neuron models are *compared* at a frequency of 32kHz. The number of time steps between the comparisons is tested with values of $2^n, n \in \{0..7\}$. The results are then evaluated according to estimate of the approximation error defined as the area between the two estimate curves

[1]Kindly provided by Felix Kern. The experimental data was collected on snail neurons for his own research and later shared to be used in this work.

with consecutive n, i.e. based on the sum of the absolute differences of voltage values at each of the time steps.

Since the single precision operations are significantly faster both on consumer graphics cards and specialized computation graphics cards, using the single precision if possible would make the method more accessible as well as increase the maximum complexity of the models that can be run in real time.

4.2.2 Results

Table 4.3 shows the differences between simulations of a stomatogastric ganglion neuron ran with different time steps for 20 seconds with random square wave current stimuli which range from 0nA to 5nA. For the rele-

	$\lvert S_{32\text{kHz}} - S_{64\text{kHz}}\rvert$		$\lvert S_{64\text{kHz}} - S_{128\text{kHz}}\rvert$		$\lvert S_{128\text{kHz}} - S_{256\text{kHz}}\rvert$		$\lvert S_{256\text{kHz}} - S_{512\text{kHz}}\rvert$	
	$\sum$	Max	$\sum$	Max	$\sum$	Max	$\sum$	Max
Single	14964mV	18.33mV	7114mV	7.44mV	3725mV	3.80mV	5019mV	34.41mV
Double	14782mV	15.75mV	7084.7mV	8.34mV	3478mV	4.22mV	1724mV	2.30mV
	$\lvert S_{512\text{kHz}} - S_{1024\text{kHz}}\rvert$		$\lvert S_{1024\text{kHz}} - S_{2048\text{kHz}}\rvert$		$\lvert S_{2048\text{kHz}} - S_{4096\text{kHz}}\rvert$			
	$\sum$	Max	$\sum$	Max	$\sum$	Max		
Single	9367mV	40.32mV	20272mV	49.41mV	43341mV	60.79mV		
Double	859mV	1.07mV	429mV	0.53mV	214mV	0.27mV		

TABLE 4.3: **Differences between numerical integrations of the STG model with different time steps for time of 20 seconds.**

vant time step settings, the time taken was measured and is presented in Table 4.4. The values were collected over 20 measurements.

	128kHz	256kHz	512kHz	1024kHz
Stomatogastric Ganglion Single precision	1291 ± 17.7ms	2279 ± 29.4ms	4223 ± 19.5ms	8127 ± 27.2ms
Stomatogastric Ganglion Double precision	5015 ± 30.9ms	11016 ± 83.1ms	21550 ± 91.1ms	42943 ± 152.0ms
Squid Giant Axon Single precision	536 ± 13.9ms	806 ± 13.9ms	1320 ± 15.5ms	2339 ± 16.0ms
Squid Giant Axon Double precision	1703 ± 31.8ms	2887 ± 35.1ms	5337 ± 27.9ms	10243 ± 39.0ms

TABLE 4.4: **Execution time of one second of simulation time for neuron simulated on a GTX 960M graphics card.**

4.2.3 Discussion

Using double precision improves the approximation error, namely for smaller time steps. This is to be expected since the error introduced by floating point operation is reduced, allowing the benefit of improved approximation error due to smaller time steps. The benefit of the double precision, however, does not seem to be significant until 128kHz therefore in the lower range it may be beneficial to use single precision for the significantly improved execution time.

Rather than the sum of (or average) of the differences, the maximum discrepancy between the approximations are more likely to be an issue when applying the error function for evaluating the performance of a candidate parametrization of a model during the estimation process. This problem does not, however, have a simple solution since the results indicate that the only possible solution is to use higher frequency double precision estimation which is not computationally feasible in real time. It is therefore necessary to account for this during the estimation process, should this ever become an issue.

An observation frequency of 4kHz (due to computational constraints) and the Euler method with a step frequency of 200kHz is used for the estimation process with single precision calculation since with this setting it is possible to execute the squid giant axon in real time[2] and the floating point operation error is not prominent factor for this step frequency.

[2]The wall time for the GPU simulation of 1 second was ~650ms on GTX 960M; ~450ms on GTX 780; and ~750ms on Tesla K40, reflecting the core clocks of ~1000MHz, 1200MHz, 810MHz, respectively. This suggests that consumer hardware may be better for real time single precision computation due to higher core clock speeds if sacrificing the neuron population size gained by higher CUDA core count is an option.

Chapter 5

Voltage Protocol Waveform Generation

5.1 Methodology

A number of methods is available when selecting a voltage or current protocol to be applied on a clamp when estimating the model parameters. Careful selection of the stimuli can help to accelerate the convergence rate of the algorithms or even fully enable the estimation of parameters of which effects would otherwise be hard to observe and distinguish. For example, certain voltage protocols were found to activate both transient and persistent currents while others will depress the transient currents, effectively isolating their effects [37].

One approach used for selecting stimuli is hand selection based on the observations made on the live cell. Such an approach proved to be effective in the past decades, however, it is hard to determine whether such a stimulus is best at distinguishing a given property and a better stimulus, which is inconsistent with previous experiences of the neuroscientist, might exist. The range of step and ramp stimuli which could be applied is wide and therefore it may be necessary to have some prior knowledge or may take long time to identify a voltage stimulus which satisfies the criteria, not to mention the number of cells necessary for making these observations.

Some works suggest to use random or semi-random voltage waveforms during the estimation process to bring out properties which might be otherwise missed on a fixed set of hand-selected stimuli. In essence, this approach is strong because the neuron is probed under wide range of circumstances and the obtained model should be more robust in a wider range of scenarios. The large stimuli variance, however, also results in application of waveforms which may not be (extensively) helpful in distinguishing the different dynamics of the neurons, resulting in an ineffective expenditure of the computational estimation time.

In order to maximize the effectiveness of the voltage protocols, an offline process is dedicated to deciding the stimuli which will be used during the real-time parameter estimation in the voltage clamp setting. Based on the assumption that little to no correlation exists between the model parameters, a set of voltage waveform protocols can be generated such that for each waveform in such set it would be possible to highlight the effect of varying one parameter while suppressing the effects of others. Since the

current is the observed variable, the optimization objective can be formulated as

$$\underset{s \in stimuli}{\operatorname{argmax}} \left(\int_{t_0}^{t_1} \left| I(s,t,p_1,..,p_f+\sigma_f,...p_n) - I(s,t,p_1,..,p_f,...p_n) \right| dt - \frac{1}{n-1} \sum_{i \in \{1..n\} \setminus f} \left(\int_{t_0}^{t_1} \left| I(s,t,p_1,..,p_i+\sigma_i,...p_n) - I(s,t,p_1,..,p_i,...p_n) \right| dt \right) \right) \tag{5.1}$$

where $stimuli$ is the set of available stimuli from which s maximizes the difference of the supplied current, $I(...)$, in the model with focus parameter p_f deviated by σ_f from the supplied current of model with parameters $p_1, ..., p_n$ while the difference for the supplied current of models with the other parameters deviated is minimized. The supplied current $I(...)$ in this is a function of time, t, the stimulus, s, and the parameters, $p_1, ..., p_n$.

The challenge of applying this method is that the true parameter set $p_1, ..., p_n$ is unknown at the time the voltage waveforms are being selected. However, it may be possible, to some extent, to select the parameters randomly from the range of parameter values in which the best parameter set is to be found. This requires the effects of the parameters to be uniform over the investigated parameter range, however same condition would have to be satisfied even if the true parameter set was known and used since otherwise the waveforms would separate the effects of parameters well around the true parameter values but the ability to separate would decrease as the parameters are deviated further from the reference $p_1, ..., p_n$ parameter set. The satisfaction of this condition largely depends on the width of range in which the parameters are estimated but also the *stability* of the model. If the model undergoes rapid changes in terms of the input-output mapping, the waveforms will inherently vary in the ability to separate the parameter effects as well.

As briefly mentioned above, this method works under the strong assumption that this approach is able to find voltage protocols which are able to highlight the effects of the different parameters or even that such protocols exist in a first place. It is, therefore, also necessary to consider that the generated stimuli will not be able to perfectly separate the parameters or that there will be high coupling between two or more parameters for that given stimulus when the stimulus is applied.

The values of σ are also unknown and need to be selected by the neuroscientist. The value should reflect the range of the given parameter but more importantly the effect the parameter has on the model. In this way, using different σ value for each parameter, rather than constant value across all parameters, helps to balance the fitness between parameters which have low impact on the behavior of the model and parameters which, when varied, fundamentally change the behaviour of the model.

The protocols are applied to the real neuron in the voltage clamp setting sequentially, focusing on estimating the parameter corresponding to the given waveform applied. The detailed description and discussion of application of the generated stimuli can be found in Chapter 6.

5.1.1 Optimization

Optimization problems, such as this one, have multiple well-established algorithms which can be used for their solution. For this problem, a genetic algorithm has been used as optimization strategy since it does not require prior knowledge about the problem and offers means to deal with local minima.

The optimization objective as defined in Eq. 5.1 requires multi-objective optimization as focus parameter, p_f, is maximized whereas the other parameters are minimized. This poses a problem with scaling of the fitnesses as introduced above along with the σ value, which is supposed to help to mitigate this issue. The σ value should, however, mainly reflect the overall effect of the parameters to perturbate them in a reasonable way and is not to be used to perfectly balance the parameter fitnesses especially since it is estimated by the neuroscientist who may have only a approximate idea about the parameter effects. The differences in scales will also alter based on the exact reference set of parameters, $p_1, ..., p_n$, that has been selected. With this being the case, the maximum change in each parameter is first found by maximizing

$$\underset{s \in stimuli}{\operatorname{argmax}} \left(\int_{t_0}^{t_1} \left| I(s,t,p_1,..,p_f+\sigma_f,...p_n) - I(s,t,p_1,..,p_f,...p_n) \right| dt \right) \quad (5.2)$$

where $\Delta_f = \int_{t_0}^{t_1} \left| I(s,t,p_1,..,p_f+\sigma_f,...p_n) - I(s,t,p_1,..,p_f,...p_n) \right| dt$ then indicates maximum deviation for any stimulus s when each parameter is perturbed on given parameter set $p_1, ..., p_n$. These maximum deviation values are then used to balance the objectives when finding the fitness by modifying Eq. 5.1:

$$\underset{s \in stimuli}{\operatorname{argmax}} \left(\int_{t_0}^{t_1} \left| I(s,t,p_1,..,p_f+\sigma_f,...p_n) - I(s,t,p_1,..,p_f,...p_n) \right| dt - \frac{1}{n-1} \sum_{i \in \{1..n\} \setminus f} \left(\frac{\Delta_f}{\Delta_i} \int_{t_0}^{t_1} \left| I(s,t,p_1,..,p_i+\sigma_i,...p_n) - I(s,t,p_1,..,p_i,...p_n) \right| dt \right) \right) \quad (5.3)$$

which helps to avoid the optimization function focusing on only one (or more) of parameter perturbations resulting in high deviations.

The voltage protocols consist of set number of voltage steps parameterized by voltage and duration. Each protocol is only observed within an observation window with set start time and variable length.

The stopping criterion was selected to depend on the percentage improvement over the past 100 iterations and limited to 500 since using absolute target fitness value as a stopping criterion would not be effective due to different scales of fitnesses for different parameters.

5.2 Results

The method was tested by optimizing 5 stimuli for both ion channel models. The total length of the stimulus was 200ms for the squid giant axon and 250ms for the stomatogastric ganglion with 3 voltage steps from -100mV

to 50mV with observation starting at 100ms and lasting from 5ms up to the end of the stimulus. These parameters reflect the stimuli used in related literature [27][37].

5.2.1 Uniformity of stimulus effects

For the squid giant axon in particular, the stimulus fitnesses varied greatly based on the initial parameters used in the different trials. This can be justified by interdependence of the parameters, especially the variables defining the internal properties of each of the ion channels and the maximum conductances: should the maximum conductance be initialized with low value, the effects of varying the sigmoid-defining variables would also have smaller effect on the overall model output. For the squid giant axon model, the possibility of using multiple models to account for this by attempting to estimate the waveforms using sum of fitnesses on multiple reference models with different parametrizations was considered as possible approach to obtain waveform with more stable effects. To contrast fitness of the generated stimuli against stimuli that may be suboptimal to fit on, a set of *degenerate* waveforms were generated by fitting for the lowest fitness possible according to Eq. 5.1.

The obtained waveforms were then tested on differently parametrized models in their ability to retain the fitness. Figure 5.1 and Figure 5.2 show the comparison of the fit stimuli against the *degenerate* stimuli for the stomatogastric ganglion and squid giant axon in terms of their fitness on parametrizations uniformly drawn from the investigated parameter range. The squid giant axon histograms also show the results for parameter estimation done using the fitness measure across 5 different parametrizations. Since lowering the fitness for the *degenerate* waveforms can be also done by drastically decreasing the observation window, the stimuli were manually inspected and this was not found the case: vast majority of the stimuli were close to the maximum observation length. This was attributed to the maximization of the parameters other than the focus parameter which results in negative fitness which involves increasing the observation length.

5.2.2 Optimized waveform

All observed stimuli optimizations were found to finish within 150 iterations showing that the improvement of the stimulus after 50 iterations was minimal ($< 10\%$).

The observation window was highly dependent on the sign of the fitness of given waveform when only the objective in Eq. 5.1 was used: stimuli with negative fitness minimized dominant effects of the non-focus parameters by shrinking the observation window to minimum (5ms) whereas the stimuli with positive fitness maximize the observed effects of the focus parameter by maximizing the observation window. This issue was mostly eliminated with the normalization introduced in Eq. 5.3 as indicated in Table 5.1 and 5.3.

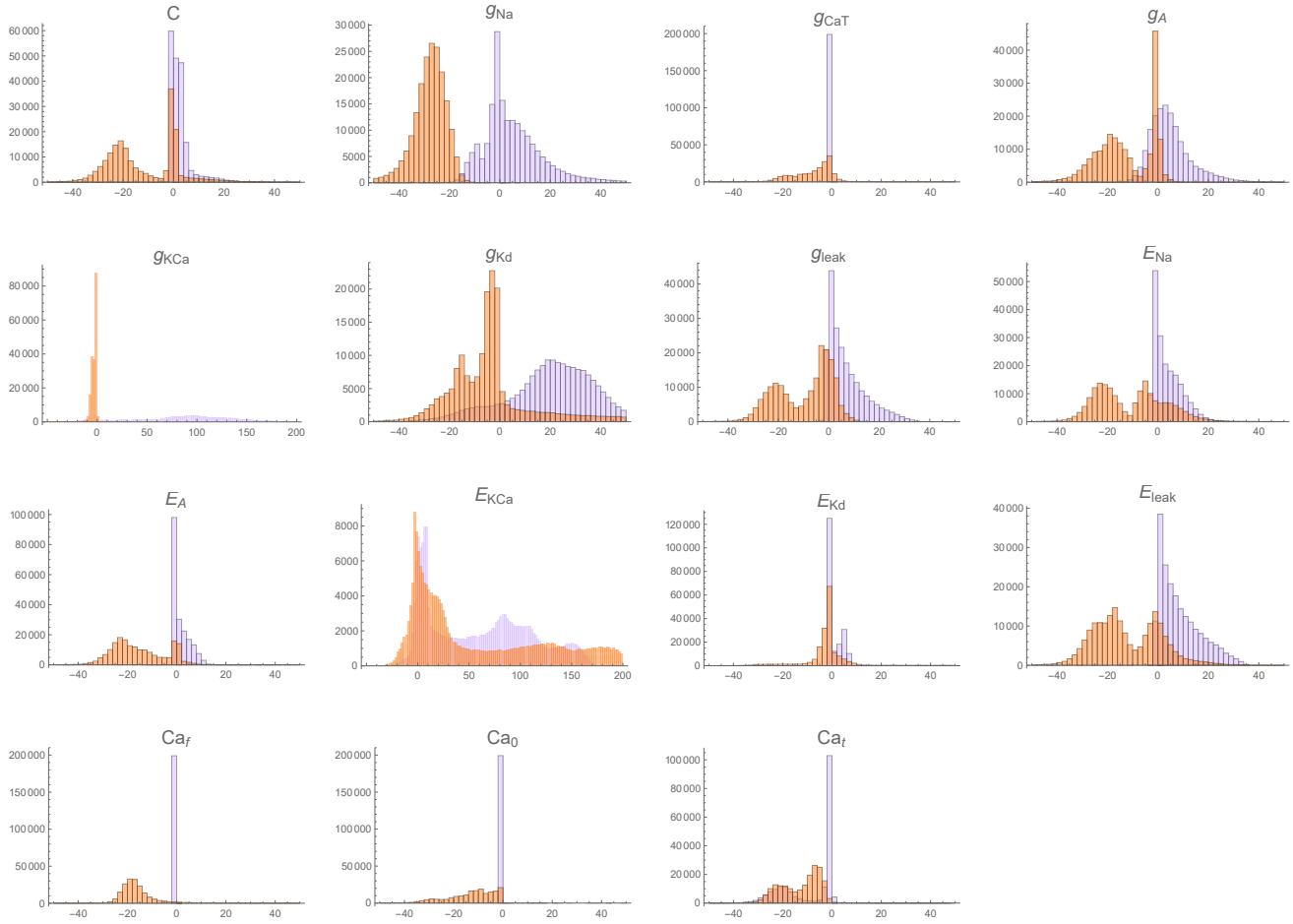

FIGURE 5.1: **Histogram of voltage waveform fitness on models with parameters drawn uniformly from the investigated parameter range on the stomatogastric ganglion model.**
Models were parametrized with sets of parameters drawn uniformly from the investigated parameters and the resulting fitnesses of the waveforms according to Eq. 5.1 have been accumulated into the histograms displayed above. The bins coloured in purple signify the results for well-optimized stimulus generated using 1 reference model; orange-coloured bins then display the fitness of the degenerate stimulus which was obtained by minimizing the fitness measure. The histograms show clear statistical difference between the fit and degenerate waveforms in terms of their fitness distribution for all parameters except E_{KCa} and E_{Kd}. Some of the well-optimized stimuli displayed positive fitness on a portion of the parametrizations, however some (Calcium concentration related parameters, g_{CaT} and E_{Kd}) display near-zero fitness for vast majority of the parametrizations, suggesting that it may not be possible to assume retention of the positive fitness on the reference model across the full parameter space.

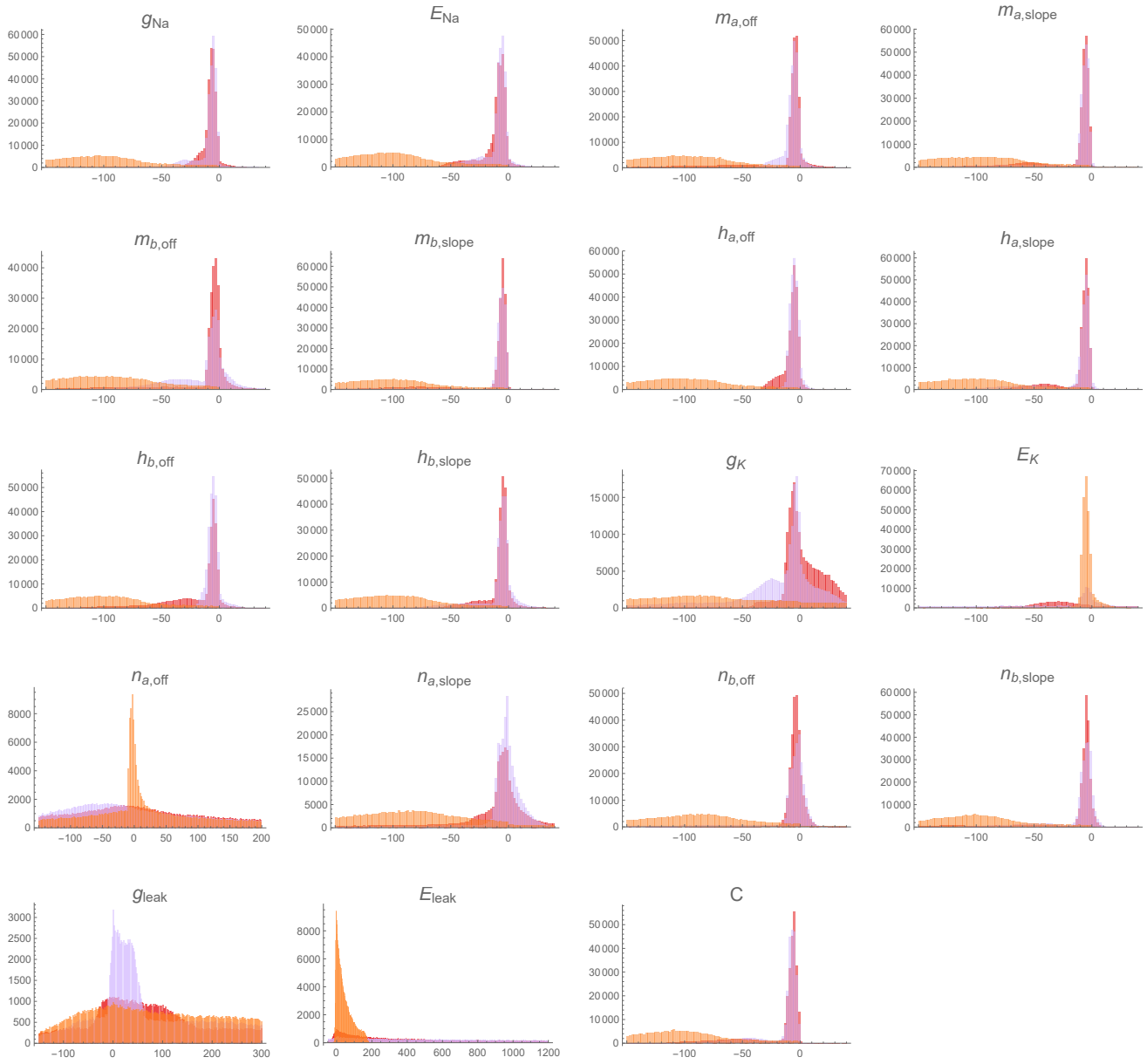

FIGURE 5.2: **Histogram of voltage waveform fitness on models with parameters drawn uniformly from the investigated parameter range for the squid giant axon model.**
Models were parametrized with sets of parameters drawn uniformly from the investigated parameters and the resulting fitnesses of the waveforms according to Eq. 5.1 have been accumulated into the histograms displayed above. Purple bins represent the fitness of a well-optimized stimulus generated using 1 reference model; red bins represent the stimulus generated using 5 reference models; and orange bins represent the degenerate stimulus which was obtained by minimizing the fitness measure. Most of the well-optimized stimuli displayed a near-zero fitness for a majority of the parametrizations which might be a direct result of small effects of some parameters compared to others on some reference parametrizations and the inability to retain fitness over wider range of parameters. Histograms display a significant statistical difference in fitness distributions between fit and degenerate waveforms, however the difference in optimization using one and five reference models is not significant.

Parameter	σ	Reference model	No normalization	With Normalization	Reference model (restricted)	No normalization
g_{Na}	0.3	32.52	-3.43	0.53	113.73	-2.73
E_{Na}	10.0	51.01	-3.47	0.22	47.66	-2.74
$m_{a,off}$	0.08	3.08	-3.48	0.148	3.32	-2.74
$m_{a,slope}$	0.2	0.12	-3.36	1.69	0.09	-2.70
$m_{b,off}$	2.0	65.64	-3.47	0.26	50.05	-2.74
$m_{b,slope}$	0.2	23.35	-3.40	0.84	18.23	-2.74
$h_{a,off}$	0.1	3.32	-3.48	0.17	3.15	-2.74
$h_{a,slope}$	0.2	17.03	-3.43	0.63	19.99	-2.73
$h_{b,off}$	0.3	3.63	-3.42	0.37	3.01	-2.74
$h_{b,slope}$	0.1	0.13	-3.44	0.60	0.08	-2.73
g_K	0.3	250.86	-0.44	99.69	234.72	-1.67
E_K	10.0	-9.53	134.76	193.39	-89.28	-0.34
$n_{a,off}$	0.03	0.97	304.62	387.96	0.63	8.09
$n_{a,slope}$	0.1	0.01	1133.32	898.4	0.01	21.44
$n_{b,off}$	2.0	53.42	0.24	164.58	59.96	-1.87
$n_{b,slope}$	0.1	53.20	-1.73	163.25	80.24	-2.05
g_{leak}	0.3	147.23	252.39	281.19	362.94	25.44
E_{leak}	10.0	-81.9	2598.09	1882.96	-47.07	835.87
C	1.0	9.67058	-3.40	1.78	4.15	-2.74

TABLE 5.1: **Resulting voltage waveform fitness of optimization on example reference model parametrization.**
The reference model was obtained by random initialization from the investigated parameter range. The restricted model was parametrized in the same way, however the range of parameters for sigmoid-defining variables was significantly decreased. When no normalization is applied, the majority of waveforms finished their optimization with negative fitness displaying that some parameters have dominant effects depending on the parametrization of the reference model. When the model was selected from the restricted parameter range for the sigmoid-defining variables, similar results were obtained (in some cases) indicating that relative values of the maximum conductances may define the scale of the effects of the individual parameters. Normalization resulted in better balance between the objectives of the optimization.

Parameter	σ	True model	No normalization
g_{Na}	0.3	120.0	64.84
E_{Na}	10.0	55.0	8.34
$m_{a,off}$	0.08	3.5	-0.02
$m_{a,slope}$	0.2	0.1	202.43
$m_{b,off}$	2.0	60.0	16.87
$m_{b,slope}$	0.2	18.0	67.41
$h_{a,off}$	0.1	3.0	-0.03
$h_{a,slope}$	0.2	20.0	44.15
$h_{b,off}$	0.3	3.0	13.18
$h_{b,slope}$	0.1	0.1	25.15
g_K	0.3	1.0	64.62
E_K	10.0	-72.0	84.87
$n_{a,off}$	0.03	0.5	53.64
$n_{a,slope}$	0.1	0.01	75.05
$n_{b,off}$	2.0	60.0	5.96
$n_{b,slope}$	0.1	80.0	59.59
g_{leak}	0.3	0.3	3.36
E_{leak}	10.0	-50.0	7.32
C	1.0	0.2	0.508

TABLE 5.2: **Resulting voltage waveform fitness of optimization on reference model parametrized with the true values for the squid giant axon model.**
Using the true model as a reference results in optimized stimuli with positive fitness for most parameters unlike for some randomly selected reference models as shown in Table 5.1.

Parameter	σ	Reference model	No normalization	With normalization	True model	No normalization
C	0.1	6.10281	171.847	225.326	0.628	0.142872
g_{Na}	3.0	608.076	968.167	904.399	283	50231.5
g_{CaT}	0.1	4.83367	-0.0606872	4.72971	3.45	1.32408
g_A	1.0	33.3832	54.0249	111.413	26.2	72.1271
g_{KCa}	3.0	181.023	3685.81	3017.11	146	4391.861
g_{Kd}	2.0	188.072	529.518	558.725	38	373.638
g_{leak}	0.05	0.861413	7.85163	8.76193	0.01	0.0410717
E_{Na}	5.0	6.15789	375.411	303.88	50	808.212
E_A	5.0	-79.8164	-0.0606937	10.203	-80	2.56664
E_{KCa}	5.0	-94.269	57.3923	193.586	-80	63.0151
E_{Kd}	5.0	-60.0191	-0.0604241	58.2874	-80	0.0270905
E_{leak}	5.0	-41.9202	15.3604	204.954	-50	0.170588
Ca_f	0.04	14.868	-0.0605603	2.55979	14.96	0.0257502
Ca_0	0.005	0.0747391	-0.0602724	0.0280663	0.05	0.0289093
Ca_t	2.0	39.6531	47.3668	430.085	200	0.303139

TABLE 5.3: **Resulting voltage waveform fitness of optimization on example and true reference model parametrization for the stomatogastric ganglion model.**
Reference model was obtained by random initialization from the investigated parameter range. When no normalization is applied, some waveforms finished their optimization with negative fitness unlike the case of true model, displaying that some parameters may have dominant effects depending on the parametrization of the reference model however this problem is not as significant as shown in Table 5.1 perhaps because of the lower interdependence of the parameters. Normalization again resulted in better balance between the objectives of the optimization.

5.3 Discussion

Figures 5.1 and 5.2 display clear differences between the fit and degenerate stimuli, showing that stimuli with inherently different effects on the scale of the full parameter range exist. However, these effects varied on different parameters, e.g. for most squid giant axon parameters the fit stimulus produces rather narrow range of fitnesses which is not true for $n_{a,off}$,E_{leak} and g_{leak}.

Even though the figures identify clear differences between fit and degenerate stimuli, the ability to retain fitness on the squid giant axon is not completely clear. Note that the fitnesses for vast majority of the examined parametrizations lie very close (and more often below) zero which poorly reflects the fitness on the reference parametrization used during the estimation process. The fitness varied greatly even on the reference stimulus depending on the reference model used for the waveform optimization as well as from parameter to parameter. This issue was more apparent for the squid giant axon likely due to higher interdependence of the parameters. When the parameter normalization introduced in Eqs. 5.2 and 5.3 was disabled, it was common for the optimization to follow the trend of majority of fitnesses being negative as indicated in Figure 5.1. On the other hand, when the true model was used for the estimation, most of the fitnesses of the waveforms reached positive values, as indicated in Table 5.2 and 5.3, which further suggests that the waveforms cannot be assumed to be uniform over the full range. It is arguable whether the relaxed parameter range might the cause of the problem in this case - when the range of the sigmoid slope and offset parameters was significantly decreased (to ± 0.25 when applicable), some reference models still produce negative fitness waveforms for some parameters as shown in Table 5.1 for "restricted". This may indicate that the relative values of the reversal potentials and the maximum conductances may be the main factors in determining the impact of the other parameters.

These issues encourage the use of co-evolution of the stimuli along with the evolving parameter set on the voltage clamp as this approach may result in better distinctive ability of the stimuli due to higher relevancy to the current parametrization rather than attempting to obtain universal stimuli beforehand. The observation of fast convergence of the fitness suggest that stimuli might be evolved fast enough for co-evolution to be applicable.

Chapter 6

Voltage Clamp Parameter Estimation

6.1 Methodology

The approach applying pre-generated waveform stimuli is in this section further investigated, continuing the work done by Thomas Nowotny. Reflecting on the results from the previous chapter on waveform generation, the possibility of co-evolving the stimuli with the estimated parameter set is investigated in this chapter as an alternative method to generating a set of universal stimuli beforehand.

6.1.1 Parameter update rule

A population of neuron models are uniformly drawn from the parameter range and updated using a genetic algorithm. The primary objective is to minimize the difference in the current injected into the real neuron and into the simulated model in order to maintain the membrane potential difference specified by the waveform and therefore the objective is to minimize the area between the curves defined by the supplied currents. Upon update, a third of a population with the highest fitness is preserved. The other two thirds are replaced by the fit individuals mutated by offsetting the parameter by a random value drawn from a Gaussian distribution with a standard deviation of σ introduced in Chapter 5 which was found to be more effective than selecting parameter uniformly from the parameter range [27]. Two parameter perturbation schemes were investigated. First mutates the parameters by adding value from Gaussian distribution of standard deviation, σ, which is different for each parameter but constant throughout the time of the estimation. Second mutates the parameters in similar way, however the standard deviation, σ, is exponentially decreasing over the time of the estimation which introduces more variance at the beginning of the estimation and allows more stable solutions at the end.

The state of the real neuron at the time of initialization is unknown which means that the real neuron and initialized models are likely to be desynchronized at the time of initialization. This issue mostly affects pacemaker neurons such as the investigated stomatogastric neuron model which produce periodical spiking behaviour even without stimulus meaning that there is constant change in opening and closing ion channels. Other neurons are affected to lesser extent since they rest at their resting potential after long enough time with no stimulus. However, this issue was not found to affect the estimation process on a voltage clamp since the internal state

of the neuron and models synchronized within tens of milliseconds after clamping them to a set voltage level. As long as the measurements are taken directly one after the other, the neuron does not a have time to desynchronize. The models were set to retain their state across generations and similarly the parent's state was copied when a mutation was produced.

The original approach suggested to sequentially cycle trough the parameters and their associated pre-generated waveforms fitting strictly one at a time under the strong assumption that the stimuli perfectly decouple the effects of the individual parameters. This effectively results in the decrease of dimensionality of the problem (provided that the parameters can be decoupled). This strong assumption was shown to not hold in all cases and therefore the non-focus parameters were allowed a chance of small mutations even when estimation was carried out using a voltage waveform protocol optimized for different parameter.

Furthermore, the original approach switched estimating different parameter if the present error was less than 80% of the running average over the past 10 iterations on that specific parameter. This would mean that any of the parameters is expected to improve the model quite rapidly at any given time and parametrization. However, this assumption does not hold when the number of the free parameters and their interdependence is increased. Limiting the number of epochs that can be spend on one parameter does resolve this issue but cycling through the parameters one at a time significantly reduces the variability of the output caused by over-fitting resulting from repetitive estimation of one parameter on a single stimulus. Eliminating the dependence of stimuli on the current state of the estimation removes the necessity to run the process in real time which can be considered advantage to this approach since not all models can be simulated in real time on present hardware.

This approach of applying stimuli has also been used in the case of estimation using co-evolved stimuli; however, in that case real-time application is still necessary as the stimuli which need to be applied to the real neuron depend on the current state of the estimation, particularly the currently most fit parametrization of the model.

6.1.2 Pre-generated waveforms

This estimation approach uses voltage waveform protocols generated offline using the methodology presented in the previous chapter. The advantage of this approach is minimal overhead of processing power during the simulation with equal performance under the assumption that the waveforms are globally optimal and do not need to be readjusted throughout the estimation process.

As previously mentioned, this approach can be also executed off-line since stimulus application does not depend on the state of the optimization.

6.1.3 Co-evolved waveforms

Generating the waveform protocols reactively to the current state of the estimation process allows for more localized stimuli which could prove to be better than global performance of the pre-generated waveforms. The elimination of the possibly long waveform optimization process prior to

the parameter estimation may also prove to be beneficial when hypothesis about the neuron needs to be quickly confirmed and iterated upon.

A population of voltage waveform protocols is randomly initialized separately for each of the parameters. The protocols are updated according to the rule specified in Chapter 5 using the most fit individual in the population of candidate neuron models as the reference. The neuron parameter estimation in turn uses the most fit and recent voltage protocol from its dedicated population.

Estimation of the next waveform based on the most recent parametrization of the model would require to alternatively run the waveform optimization and parameter estimation in sequence. This approach would consume a valuable time of the cell life and the internal state of the observed cell would desynchronize each time the waveforms would be optimized. The waveform optimization is therefore done in parallel to the parameter estimation on a second GPU with the minor disadvantage of using the second most recent parameter set as its reference. This has, however, only a minor impact since the local performance of the protocols is significantly more consistent than the global performance and the parameter change from one epoch to the next decreases with advancing time of the estimation.

6.2 Results

Table 6.1 shows the results for different stimuli application approaches in the form $Average \pm Standard\ deviation$ for the squid giant axon. For the estimation approach using random stimuli, a new stimulus was generated each epoch. The generated waveforms lasted 200ms with observation window beginning at 100ms and lasting $50 - 100\text{ms}$ with 3 voltage steps which range from -100mV to 50mV. Same values were used for generation of both the pre-generated and the co-evolved waveforms with the exception of minimum observation length being 5ms.

Similarly, Table 6.2 shows the results for the stomatogastric ganglion model with generated waveforms being 250ms long with 3 steps within the range of -100mV to 50mV and observation window starting at 100ms of minimum length of 5ms for pre-generated waveform protocols, 50ms for random protocols and maximum length of 150ms for both.

The estimation was executed within the range and with 'true model' as indicated in the tables. The population of the candidate model was initialized randomly from the indicated range and in all of these experiments had size of 4000 (maximum that was found to run fully in parallel, larger sizes resulted in increased computation time on NVIDIA GTX 780). For both the squid giant axon and stomatogastric ganglion, 60 trials were executed with distinct initial populations and with varying waveforms for each of the observed stimuli application approaches. The initializations were consistent across the stimuli approaches. Each of the trials was executed with total observation time of 15minutes.

The standard deviations of the parameter perturbations, σ, are indicated in Tables 5.1 and 5.3 for the trials with parameter perturbations using constant standard deviation. For the trials with decreasing parameter perturbations, the standard deviation of the perturbation at time t was computed with exponential falloff as $\sigma_t = 8 \times 0.9994^{0.005\sigma}$ resulting in starting values

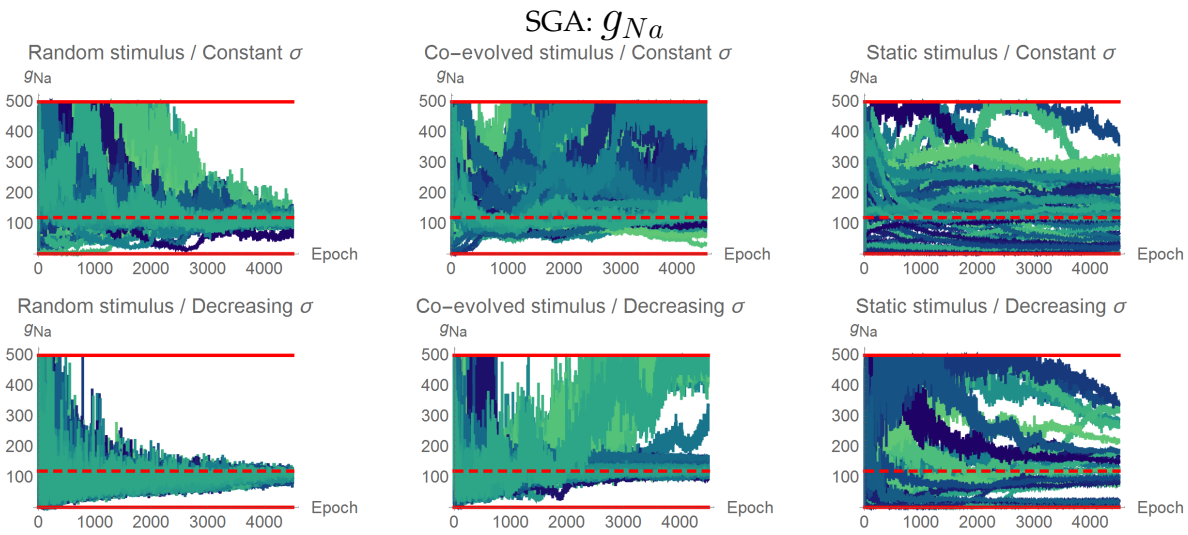

FIGURE 6.1: **Progress of voltage clamp estimation for all estimation schemes on the squid giant axon model.**
Multiple trials with randomly initialized populations have been executed with each optimization strategy ran for 15 minutes each. The displayed plots show the value of g_{Na} for a best candidate in each epoch with different colours for each run. Using decreasing σ improves the convergence for all of the estimation strategies. Some runs of estimation with co-evolved stimulus diverge in their value which is characteristic for this method. Results for estimation with static stimulus show improvement, however the time to converge is higher.

of 800% and finishing value (at 15 minutes) of 53.7% of those indicated in the appropriate table for the σ constants. The trials using random stimuli to estimate parameters for the stomatogastric ganglion neuron were observed to produce unstable candidate models even in trials with constant σ, as can be seen in Figure 6.2, and therefore the falloff for those trials was defined as $\sigma_t = 1 \times 0.9994^{0.005\sigma}$.

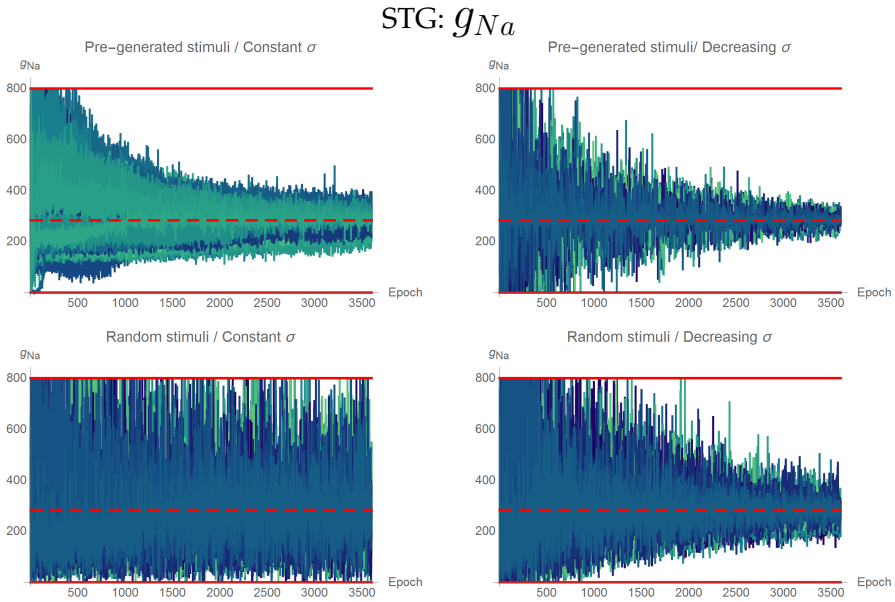

FIGURE 6.2: **Progress of voltage clamp estimation for estimation schemes using the pre-generated and random on the stomatogastric ganglion model**
Multiple trials with randomly initialized populations have been executed with each of the optimization strategies ran for 15 minutes each. The displayed plots show the value of g_{Na} for a best candidate in each epoch with different colours for each run. Pre-generated stimulus shows clear convergence both with constant and decreasing σ although decreasing σ allows for a slight improvement and on random stimulus enables convergence altogether.

Constant σ						
Parameter	Min	Max	True	Random	Co-Evolved	Pre-generated
g_{Na}	1.0	500.0	120.0	$\mathbf{114.0 \pm 11.4}$	224.8 ± 154.2	139.3 ± 80.9
E_{Na}	0.0	100.0	55.0	$\mathbf{57.0 \pm 4.8}$	60.1 ± 14.1	57.2 ± 21.4
m_{aoff}	2.5	4.5	3.5	$\mathbf{3.47 \pm 0.38}$	3.9 ± 0.5	3.9 ± 0.41
m_{aslope}	0.06	0.14	0.1	$\mathbf{0.0967 \pm 0.0103}$	0.0790 ± 0.0206	0.0834 ± 0.0226
m_{boff}	50.0	70.0	60.0	$\mathbf{58.0 \pm 2.3}$	64.6 ± 6.0	59.5 ± 6.4
$m_{bslop}e$	12.0	24.0	18.0	$\mathbf{16.5 \pm 2.1}$	20.7 ± 3.7	18.3 ± 4.5
h_{aoff}	2.0	4.0	3.0	$\mathbf{3.40 \pm 0.38}$	2.76 ± 0.70	2.86 ± 0.73
h_{aslope}	12.0	28.0	20.0	$\mathbf{18.5 \pm 2.9}$	17.7 ± 3.7	18.4 ± 4.4
h_{boff}	2.0	4.0	3.0	$\mathbf{3.03 \pm 0.41}$	3.65 ± 0.46	3.25 ± 0.76
h_{bslope}	0.06	0.14	0.1	$\mathbf{0.102 \pm 0.010}$	0.083 ± 0.024	0.097 ± 0.026
g_K	1.0	500.0	36.0	$\mathbf{37.8 \pm 2.3}$	152.1 ± 137.4	160.8 ± 124.9
E_K	-100.0	0.0	-72.0	$\mathbf{-72.0 \pm 0.7}$	-60.5 ± 22.7	-49.0 ± 27.5
n_{aoff}	-0.5	1.5	0.5	$\mathbf{0.492 \pm 0.016}$	0.129 ± 0.348	0.104 ± 0.317
n_{aslope}	0.006	0.014	0.01	$\mathbf{0.00985 \pm 0.00035}$	0.00975 ± 0.00234	0.00844 ± 0.00261
n_{boff}	50.0	70.0	60.0	$\mathbf{58.2 \pm 2.8}$	54.4 ± 4.2	56.0 ± 5.4
n_{bslope}	48.0	112.0	80.0	$\mathbf{88.4 \pm 9.2}$	95.7 ± 20.7	96.8 ± 22.2
g_{leak}	0.1	500.0	0.3	$\mathbf{0.300 \pm 0.006}$	8.424 ± 8.443	6.763 ± 7.426
E_{leak}	-100.0	0.0	-50.0	$\mathbf{-49.8 \pm 1.2}$	-73.4 ± 21.3	-78.4 ± 21.5
C	0.1	10.0	1.0	$\mathbf{0.96 \pm 0.43}$	1.13 ± 0.42	0.77 ± 0.45
Decreasing σ						
Parameter	Min	Max	True	Random	Co-Evolved	Pre-generated
g_{Na}	1.0	500.0	120.0	$\mathbf{106.9 \pm 9.6}$	143.0 ± 77.1	138.9 ± 92.2
E_{Na}	0.0	100.0	55.0	61.2 ± 4.3	$\mathbf{55.0 \pm 1.8}$	62.3 ± 18.7
m_{aoff}	2.5	4.5	3.5	3.1 ± 0.3	$\mathbf{3.6 \pm 0.5}$	3.9 ± 0.5
m_{aslope}	0.06	0.14	0.1	0.0858 ± 0.0078	$\mathbf{0.0994 \pm 0.0159}$	0.0973 ± 0.0174
m_{boff}	50.0	70.0	60.0	56.2 ± 1.7	$\mathbf{60.7 \pm 3.4}$	54.7 ± 4.7
$m_{bslop}e$	12.0	24.0	18.0	15.4 ± 1.1	$\mathbf{18.8 \pm 2.8}$	18.7 ± 3.0
h_{aoff}	2.0	4.0	3.0	3.47 ± 0.18	$\mathbf{3.01 \pm 0.67}$	$\mathbf{3.10 \pm 0.56}$
h_{aslope}	12.0	28.0	20.0	16.6 ± 1.2	$\mathbf{20.4 \pm 4.1}$	20.8 ± 4.1
h_{boff}	2.0	4.0	3.0	$\mathbf{2.77 \pm 0.20}$	3.2 ± 0.45	3.42 ± 0.55
h_{bslope}	0.06	0.14	0.1	$\mathbf{0.094 \pm 0.005}$	0.100 ± 0.013	0.103 ± 0.015
g_K	1.0	500.0	36.0	$\mathbf{37.0 \pm 0.6}$	45.4 ± 39.3	128.3 ± 91.7
E_K	-100.0	0.0	-72.0	$\mathbf{-72.1 \pm 0.5}$	-69.5 ± 12.9	-64.0 ± 16.9
n_{aoff}	-0.5	1.5	0.5	0.493 ± 0.007	$\mathbf{0.459 \pm 0.177}$	0.227 ± 0.244
n_{aslope}	0.006	0.014	0.01	$\mathbf{0.00990 \pm 0.00014}$	0.01017 ± 0.00042	0.00716 ± 0.00186
n_{boff}	50.0	70.0	60.0	$\mathbf{59.4 \pm 1.0}$	57.6 ± 5.1	60.6 ± 4.6
n_{bslope}	48.0	112.0	80.0	$\mathbf{86.5 \pm 3.6}$	79.4 ± 13.4	102.4 ± 18.6
g_{leak}	0.1	500.0	0.3	$\mathbf{0.299 \pm 0.004}$	1.50 ± 4.59	0.35 ± 0.20
E_{leak}	-100.0	0.0	-50.0	$\mathbf{-49.9 \pm 0.75}$	-53.0 ± 11.5	-53.1316 ± 8.90409
C	0.1	10.0	1.0	0.59 ± 0.29	$\mathbf{1.10 \pm 0.35}$	0.90 ± 0.46

TABLE 6.1: **Voltage clamp estimation results for co-evolved, pre-generated and random stimuli with constant and decreasing σ values for the squid giant axon.**
Estimation with constant σ values allows the random stimulus to perform better than the schemes using pre-generated and co-evolved stimuli. Values in bold indicate best fit for given parameter. With decreasing σ the co-evolved stimuli perform better on some parameters, suggesting that higher variance in the population promoted by higher σ values at the beginning of the estimation beneficial.

Parameter	Min	Max	True	Random	Pre-generated	Random Decreasing σ	Pre-generated Decreasing σ
C	0.100	10.000	0.628	$\mathbf{0.889 \pm 0.139}$	0.911 ± 0.151	0.882 ± 0.134	$\mathbf{0.698 \pm 0.058}$
g_{Na}	0.0	800.0	283.0	296.3 ± 69.0	$\mathbf{305.6 \pm 21.0}$	283.7 ± 26.3	$\mathbf{291.1 \pm 17.1}$
g_{CaT}	0.00	5.00	3.45	$\mathbf{3.16 \pm 0.53}$	2.95 ± 0.49	3.09 ± 0.51	$\mathbf{3.29 \pm 0.22}$
g_A	0.0	75.0	26.2	25.5 ± 8.8	$\mathbf{28.8 \pm 2.3}$	26.4 ± 9.1	$\mathbf{25.6 \pm 4.9}$
g_{KCa}	0.0	300.0	146.0	145.2 ± 7.57	$\mathbf{147.0 \pm 2.8}$	147.2 ± 5.3	$\mathbf{146.8 \pm 0.6}$
g_{Kd}	0.0	200.0	38.0	45.8 ± 20.0	$\mathbf{41.0 \pm 4.1}$	45.6 ± 17.2	$\mathbf{38.1 \pm 2.5}$
g_{leak}	0.000	1.000	0.010	$\mathbf{0.010 \pm 0.001}$	0.016 ± 0.009	0.010 ± 0.009	$\mathbf{0.010 \pm 0.000}$
E_{Na}	0.0	100.0	50.0	50.7 ± 3.0	$\mathbf{49.0 \pm 0.7}$	50.2 ± 1.3	$\mathbf{49.8 \pm 0.6}$
E_A	-100.0	0.0	-80.0	-73.8 ± 17.0	$\mathbf{-72.2 \pm 5.8}$	-73.0 ± 14.6	$\mathbf{-77.0 \pm 10.8}$
E_{KCa}	-100.0	0.0	-80.0	-79.9 ± 0.6	$\mathbf{-79.9 \pm 0.2}$	-80.0 ± 0.4	$\mathbf{-79.9 \pm 0.2}$
E_{Kd}	-100.0	0.0	-80.0	-73.4 ± 9.6	$\mathbf{-75.7 \pm 7.7}$	-67.4 ± 17.8	$\mathbf{-79.8 \pm 1.8}$
E_{leak}	-100.0	0.0	-50.0	$\mathbf{-49.5 \pm 1.3}$	-59.4 ± 11.6	-48.9 ± 5.2	$\mathbf{-49.7 \pm 0.9}$
Ca_f	14.00	16.00	14.96	$\mathbf{15.08 \pm 0.54}$	15.39 ± 0.58	$\mathbf{15.06 \pm 0.68}$	14.39 ± 0.38
Ca_0	0.010	0.100	0.050	0.056 ± 0.025	$\mathbf{0.051 \pm 0.026}$	0.053 ± 0.030	$\mathbf{0.049 \pm 0.026}$
Ca_t	20.0	250.0	200.0	$\mathbf{196.6 \pm 51.6}$	162.2 ± 37.0	$\mathbf{200.6 \pm 19.4}$	177.2 ± 25.6

TABLE 6.2: **Voltage clamp estimation results for pre-generated and random stimuli with constant and decreasing σ values for the stomatogastric ganglion.**
Values in bold indicate best fit for given parameter. With constant σ values, the strategy using pre-generated stimuli outperforms strategy with random stimuli on some parameters and the performance is further improved with decreasing σ.

6.3 Discussion

The results on the squid giant axon clearly suggest against the theory that pre-generated waveforms are uniformly applicable over the inspected range of the parameters. Upon close inspection, the generation of the waveforms was dominated by several parameters that seemed to have large effect on the output whereas the rest of the parameters had negligible effects resulting in waveforms that were not able to sufficiently decouple the focused parameter even with normalization as indicated in the previous chapter. The resulting observations may have offered very little information about the performance of the model. Throughout the estimation, the waveforms which were found to impact the model in very limited way during the waveform optimization displayed error ratings significantly closer to the noise level than those that were found to produce large changes which further suggests low contribution to the estimation process. This may be one of the contributing factors of low performance of the pre-generated stimuli on the squid giant axon model both with constant and decreasing σ values.

Allowing for higher initial σ values and exponentially decreasing them throughout the time of the estimation appears to have a positive effect on the ability to converge to the correct solution. This may indicate that the used optimization method with fairly homogeneous population resulting from replication of the elite population with small sigma values is not sufficient for traversing the error landscape likely due to presence of large local minima which the algorithm fails to escape. These may be a direct result of correlation between the parameters, mainly of the sigmoid-defining variables of the individual ion channels. The improvement seen with decreasing σ is then natural since the algorithm is forced to more generalized search at the beginning of the estimation. The improvement seen in using random stimuli compared to the pre-generated stimuli may also partly be a product of this problem since the variance of the best candidate over time of the estimation was higher than for pre-generated stimulus which also indicates less homogeneous elite population resulting in less localized search, as seen in Figure 6.1.

Co-evolved stimuli appear to outperform the random stimulus on some parameters with decreasing σ, however variances of results on some parameters such as the conductances and reversal potentials seem to be high. The stimuli generated along with the estimation of the parameters seemed to be better at retaining their positive fitness, mostly eliminating the issues tied to generating universal stimuli based on a randomly parametrized model discussed in the previous chapter. Taking into account that the co-evolution method is likely to still be affected by the issue of a too homogeneous population, it is likely to be the best performing method if these problems are resolved. It, however, seems to be the case that repeated stimulation of a cell greatly reduces its life time[1] which may render this method physiologically unfeasible or to some extent limited. The extent of this issue still remains to be found and may be of interest if this method is subject to future investigation.

The parameter estimation of the stomatogastric ganglion model with pre-generated stimuli have shown to be more consistent and accurate on

[1] Information provided casually by Felix Kern based on observations during his ongoing unpublished research.

some parameters than when random stimuli are used in cases of both the constant and decreasing σ approach. This may be because of the higher quality of the stimuli as seen in the previous chapter. As opposed to the stimuli for the squid giant axon model, which are mostly very near zero fitness when uniformly tested across the parameter range, the stimuli for the stomatogastric ganglion model have often shown to extend into the positive fitness values as well, indicating higher ability to separate the effects of individual parameters which likely contributes to the improved performance.

Due to a likely smaller correlation between the parameters in the stomatogastric ganglion model, the localized search of the pre-generated stimuli does not appear to be as problematic in this case because of apparent lack of un-escapable local minima. Since the estimation method have shown an ability to converge toward a single (correct) solution for most of the parameters in the case of the stomatogastric ganglion, the improvement posed by using decreasing σ as opposed to constant ones may be result of the sped-up convergence at the beginning (by higher σ values) and decreased best model candidate variance (caused by lower σ values) towards the end as seen in Figure 6.2.

The original prototype proposed by Thomas Nowotny, which uses same optimization strategy, have displayed an ability to rapidly converge for all of the estimated parameters and then track small changes over time. The results found here are consistent with the original results; however, in the original work, the complexity of the problem was significantly lower and the problem was slightly idealized (see Section 2.11) which allows the original method to rapidly converge using the diversity of the randomly initialized population before the elite population becomes uniform and then continue to track small changes in the variables with the very uniform population. Due to the aforementioned issues and higher combinatorial complexity of the above explored settings, the results presented here are significantly different form the original work, indicating that the assumptions which held in that simpler, idealized scenario may be still true for more complex settings but not to the full extent.

Chapter 7

Current Clamp Parameter Estimation

The addition of current clamp introduces the ability to refine the parameters obtained on a voltage clamp which obtains only approximate parameter sets but is unable to find the best settings due to the shallow fitness landscape and noisy readings. Current clamp complements these features with a fitness landscape which is not nearly as shallow but contains significantly more local minima as indicated in Figure 7.1.

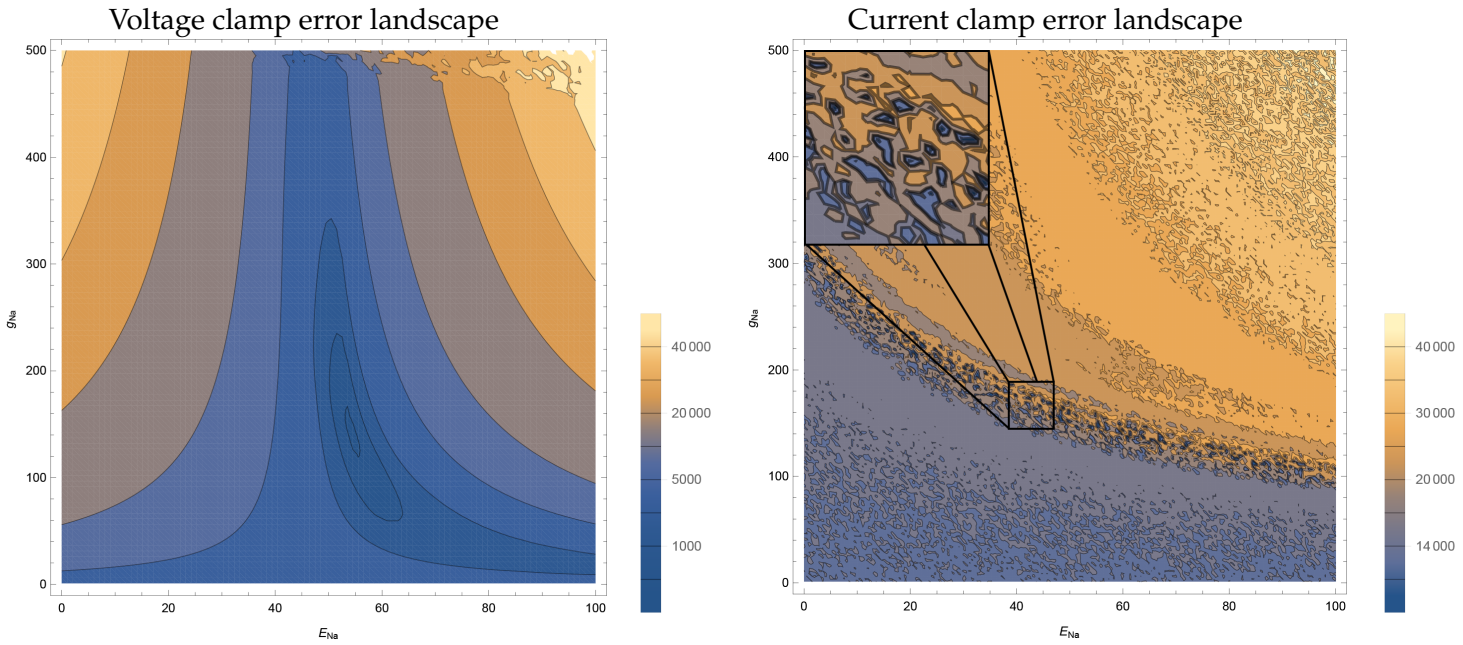

FIGURE 7.1: **Difference in the error landscapes of voltage and current clamp for varying g_{Na} and e_{Na} parameters in the squid giant axon neuron model.**

7.1 Methodology

In a current clamp setting, a varying current is injected into the cell and the voltage potential response is observed. The membrane potential response of a real neuron is characteristic in the production of action potentials - brief depolarizations of the membrane potential. This renders the method of simply taking the area between the output of the reference neuron and the estimated model as an insufficient measure of fitness since any slight

shift in the phase of the neuron can produce massive decrease in the fitness of that neuron model even if the response is otherwise identical. The voltage outputs of the observed neuron and the computer model are therefore coupled by complementing the model output with the output observed in the real cell:

$$V = (1.0 - k)(V_0 + \frac{\Delta V}{\Delta t}) + k(V_{recording}) \tag{7.1}$$

Where V is the updated membrane potential, V_0 is membrane potential at previous iteration in the candidate model and $\frac{\Delta V}{\Delta t}$ is the update in the potential in the current time step. $V_{recording}$ is the membrane potential recorded in the live neuron and $k \in [0.0, 1.0]$ is the coupling variable which defines the extent to which the cells are coupled. The coupling is initiated at $k = 1.0$ and decreases with exponential falloff throughout the estimation process until the cells are fully decoupled at a later time of the estimation.

Application of the coupling allows the area between the two voltage output curves to act as a sufficient indicator of a fitness. Using sum of absolute differences at observed times (L1) performed significantly better than sum of squares (L2) error measure. L2 accounts higher importance to large differences which happens almost exclusively in action potential intervals and the resulting estimated models were good at reproducing the action potentials of the exact amplitude as the reference neuron but were not as good at reproducing the spike after-hyper-polarization. Using L1 generally solved this issue and the spike amplitude reproduction was not noticeably impacted. The significant maximum difference in the numerical approximations observed in Chapter 4 may have contributed to this issue as well. Extending the observation to cover at least two spikes (or pacemaker potentials in the STG) seemed to further improve the ability to accurately estimate the spiking frequency as it is easier to identify the correct spiking rate.

As mentioned, the problem of the initialization is the high probability of desynchronisation between the real neuron state and the simulated models. The issue is resolved similar to voltage clamp: the observations are made successively and the internal state of the candidate models is always preserved both on the replication and the mutation. Since the state was synchronized after the voltage clamp is finished, the current clamp estimation can be executed directly after and the internal state of the selected model candidate in the voltage clamp setting can be used to initialize the population on the current clamp. The retained synchronization between the states of the real neuron and the simulated models is also supported by the coupling introduced above, by retaining the membrane potential at a level similar to the live cell and thus inducing similar environment for the voltage-dependent ion channel activation.

In case of the parameter estimation in the current clamp setting, generating a set of universal stimuli is not a viable option. First, when a set of stimuli was generated using the model estimated in the voltage clamp setting, it was found to quickly lose its separating properties even in immediate neighbourhood of the used model in the parameter space. Second, since the parameter estimation in voltage and current clamp setting is done in immediate succession, there is no extensive amount of time to pre-generate the stimuli. The parameters were therefore estimated together without attempt to separate their effects. Using a random current step stimuli have

been found to be sufficient for refining the parameters from current clamp, however co-evolving the stimuli according to the objective specified in the Eq. 5.2 while cycling through the focus parameters yields 50% increase in the objective fitness value compared to the random stimuli even when accounting for the one epoch delay discussed in Section 6.1.3. It is, however, arguable whether selecting stimuli in this way brings any benefit to the parameter estimation performance since no tangible difference was observed when this technique was applied.

7.2 Results

Consistent pre-generated sets of stimuli were used to estimate parameters in the voltage clamp setting for reference models indicated in Table 7.1. These models were used by Golowasch et. al. to demonstrate the different parameter sets producing very similar physiological behavior [1]. The voltage clamp estimation outputs were then used for current clamp estimation with the results shown in Table 7.1 in the form $AVG \pm SD$ for 30 trials. A sample of the estimated model for each of the reference models is shown in Figure 7.2.

			(A)		(B)		(C)	
Parameter	Min	Max	True	Estim.	True	Estim.	True	Estim.
C	0.1	10.0	0.628	0.629 ± 0.005	0.628	0.628 ± 0.007	0.628	0.615 ± 0.074
g_{Na}	0.0	800.0	**400.0**	452.7 ± 73.3	**50.0**	52.7 ± 9.7	**50.0**	50.1 ± 10.3
g_{CaT}	0.0	5.0	4.0	3.8 ± 0.2	4.0	3.8 ± 0.2	4.0	3.9 ± 0.2
g_A	0.0	75.0	5.0	8.3 ± 2.1	5.0	8.1 ± 3.0	5.0	6.2 ± 2.3
g_{KCa}	0.0	300.0	250.0	246.4 ± 6.9	250.0	249.1 ± 10.1	250.0	250.5 ± 7.1
g_{Kd}	0.0	200.0	**20.0**	20.2 ± 2.3	**20.0**	26.7 ± 4.8	**100.0**	103.1 ± 13.6
g_{leak}	0.0	1.0	0.010	0.010 ± 0.004	0.010	0.012 ± 0.005	0.010	0.012 ± 0.007
E_{Na}	0.0	100.0	50.0	43.9 ± 9.3	50.0	46.9 ± 14.3	50.0	45.8 ± 11.4
E_A	-100.0	0.0	-80.0	-52.5 ± 13.7	-80.0	-51.2 ± 22.4	-80.0	-51.1 ± 29.1
E_{KCa}	-100.0	0.0	-80.0	-80.6 ± 1.0	-80.0	-80.0 ± 1.2	-80.0	-80.3 ± 0.8
E_{Kd}	-100	0.0	-80.0	-80.7 ± 10.4	-80.0	-68.6 ± 15.3	-80.0	-82.5 ± 7.2
E_{leak}	-100.0	0.0	-50.0	-51.5 ± 2.6	-50.0	-51.7 ± 3.1	-50.0	-50.7 ± 4.7
Ca_f	14.00	16.00	14.96	15.4 ± 0.5	14.96	15.64 ± 0.26	14.96	15.49 ± 0.29
Ca_0	0.010	0.10	0.050	0.043 ± 0.024	0.050	0.038 ± 0.019	0.050	0.040 ± 0.025
Ca_t	20.0	250.0	200.0	194.6 ± 8.8	200.0	196.8 ± 6.3	200.0	195.8 ± 9.0

TABLE 7.1: **Current clamp estimation results for 3 models of the stomatogastric ganglion with varying parameters but very similar spiking behaviour.**
The joint procedure of using voltage clamp followed by current clamp for parameter estimation shows clear ability to distinguish between models with similar spiking behaviour (displayed in Fig. 7.2) but varying parameters (shown in bold). The data shown is based on 30 trials with distinct parameter initializations for each of the models.

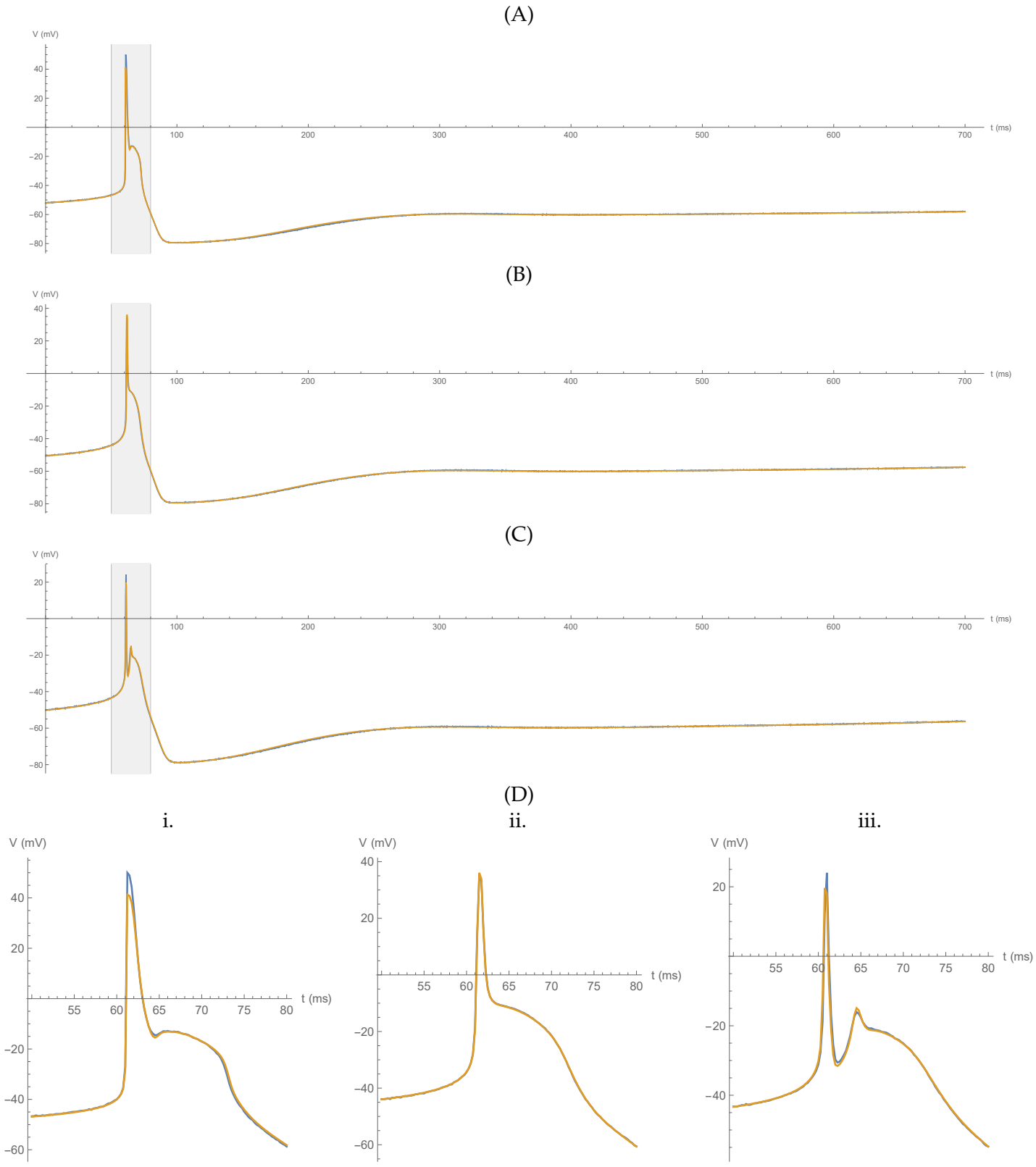

FIGURE 7.2: **Performance of the estimated model for the stomatogastric ganglion with no current is applied**. Blue shows the reference neuron and yellow shows the estimated model. Subfigures A-C correspond to results in Table 7.1, Subfigures D:i-iii focus on highlighted regions in Subfigures A-C, respectively. The investigated method has shown ability to reproduce the very similar behaviour of the 3 reference models despite the variation in parameter values.

7.3 Discussion

The results presented in Table 7.1 show a clear ability of the method combining the voltage and current clamp to differentiate between models with vast variance in some parameters but very similar physiological behaviour. Since methods producing comparable or even better results has been proposed in the past (such as those mentioned in Related Research), it is highly unlikely that differences of parameters at this scale would be unnoticed if they were, actually, present in real neurons. Averaging should, therefore, never pose a problem at this scale since state-of-the-art parameter estimation methods are accurate enough to clearly indicate the difference between these different parametrizations, at least in the investigated case. Should a problem with averaging on same parameters ever arise (with smaller scale differences such as when both $\overline{g}_{Kd}$ and $\overline{g}_{Na}$ are high, Figure 2.3), it may indicate an instability of the proposed model rather than cell-to-cell variation. While distinct regions on large scale are desirable, indicating clear differences resulting from varying the parameters, large differences with small parameter changes in the model would indicate large differences in the physiological behaviour of the neuron with small changes in the structure which is not likely to be the case.

Chapter 8

Conclusion

The investigated method has been shown to correctly distinguish between different parametrizations of the stomatogastric ganglion neuron model even in cases where significantly varying parametrizations display very similar spiking behaviour. The ability of the estimation in the voltage clamp setting to obtain approximate solutions likely contributes to the observed performance, however it was found that for more complex parameter estimation tasks the investigated voltage clamp estimation approach was not able to converge to the true solution. This seems to be especially the case for tasks with multiple unknown parameters such as the squid giant axon model with unknown conductances, reversal potentials and slopes and offsets of the channel-defining sigmoids. While this problem may be improved upon or even be solved by more suitable optimization strategy, it may also be valid approach to assume the internal parameters of the ion channels to remain constant (since variance would likely mean variance in the structure of the membrane proteins as well) and carry out the parameter estimation on the conductances which has been shown to be significantly less challenging. Since the parameters defining the sigmoids (and therefore the dynamics of individual channels) are unlikely to vary between neuron (since that would mean varying structure of the ion channels), the sigmoids may be estimated using the strategies employing blockers to isolate the estimated parameters on the real neuron.

While the method was found to be able to operate in real time for simple cells (such as the squid giant axon), the complexity of the computation increases with additional channels of cells which are of higher interest in modern research. It has been shown, however, that repeated stimulation of the cell in the voltage clamp setting may lead to significant decrease of the life of the cell[1] which would render approaches relying on on-line stimulus adjustment (such as the co-evolution approach) unusable.

8.1 Further investigation

This work focuses mostly on the investigation of the process of using waveforms potentially able to decouple parameter to increase fitting performance and many areas remain insufficiently explored. One major problem is the selection of the correct optimization strategy. A very simple genetic algorithm-like strategy which preserves elites within the population and creates offspring by a simple mutation operator resulted in rather homogeneous populations which seemed to be problematic for estimation. There is a wide range of optimization algorithms both within and outside of the family

[1] Felix Kern, private communication

of genetic algorithms. The use of a better optimization strategy may improve the performance as discussed in Section 6.3 and allow the estimation method to better capitalize on the potential benefits of parameter separation in some estimation scenarios with more complex error surfaces.

It has been shown that increased variance in the population leads to better performance in some cases. The by-product of the increase in population variance is possible increase in the instability of the solution as seen in Figure 6.2. It may be necessary to consider using results from estimation using two or more waveforms to decide whether a given model candidate should be accepted into the elite population or similar approach to obtain more stable solution while conserving population diversity.

The problem of stopping conditions is not considered in this work since a constant time budget is considered as a single constraint. It may be beneficial to explore the possibility of more flexible stopping condition which may benefit both estimation in real-time and off-line.

Finally, the original method has shown the ability to track drifting parameters over the time in a simple setting in the voltage clamp setting. Since repeated voltage clamping have shown to lead to faster death of (some) cells as previously mentioned, it may be impossible to track the cell for longer time periods, current clamp may be more suitable for this purpose from physiological standpoint, however computational applicability remains to be unexplored.

Appendix A

Stomatogastric ganglion voltage clamp convergence

Figures in this appendix display the values for all parameters of the best candidate model changing over the time course of the parameter estimation. Multiple runs are displayed in each figure, indicated by distinct colours.

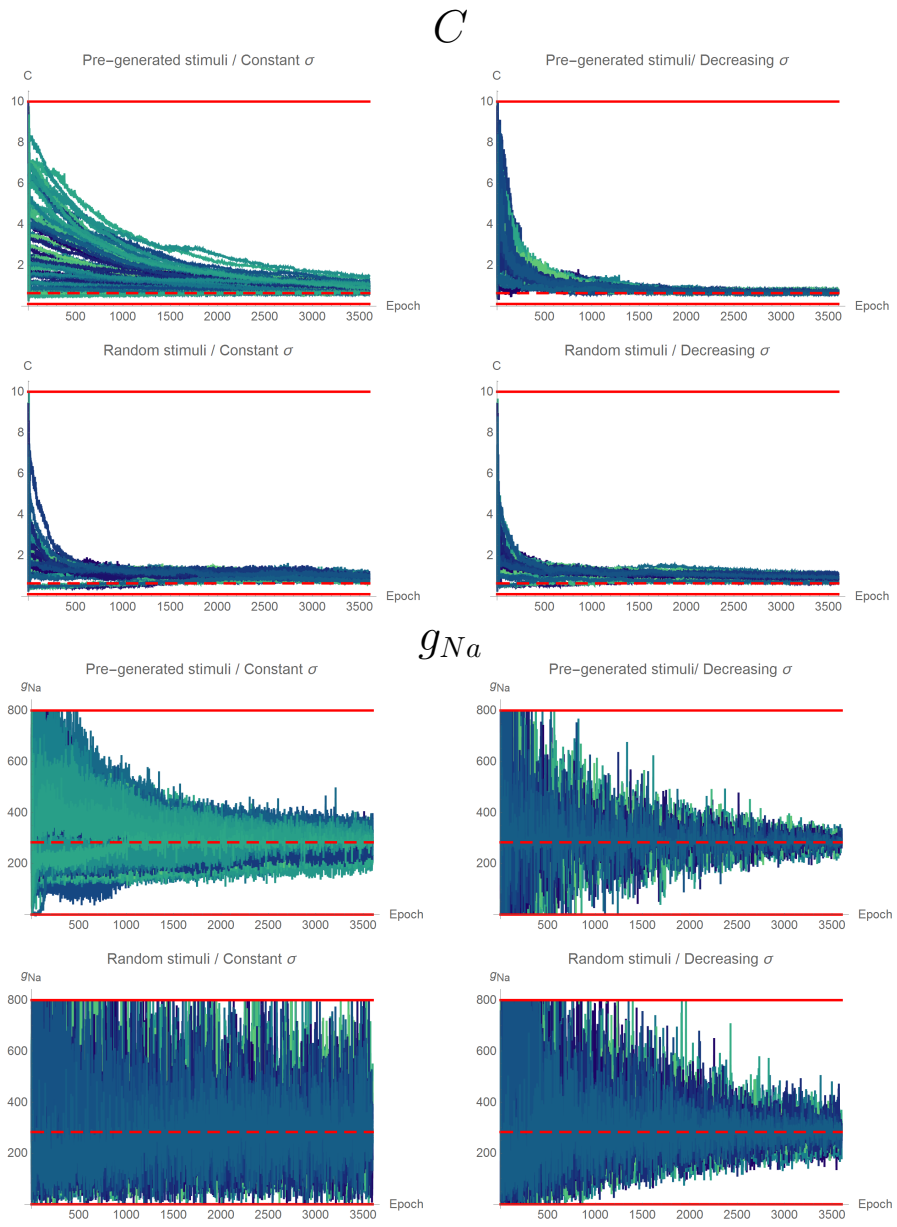
C
Pre−generated stimuli / Constant σ
Pre−generated stimuli/ Decreasing σ
Random stimuli / Constant σ
Random stimuli / Decreasing σ
C
10
8
6
4
2
500 1000 1500 2000 2500 3000 3500
Epoch
g_{Na}
Pre−generated stimuli / Constant σ
Pre−generated stimuli/ Decreasing σ
Random stimuli / Constant σ
Random stimuli / Decreasing σ
g_{Na}
800
600
400
200
500 1000 1500 2000 2500 3000 3500
Epoch

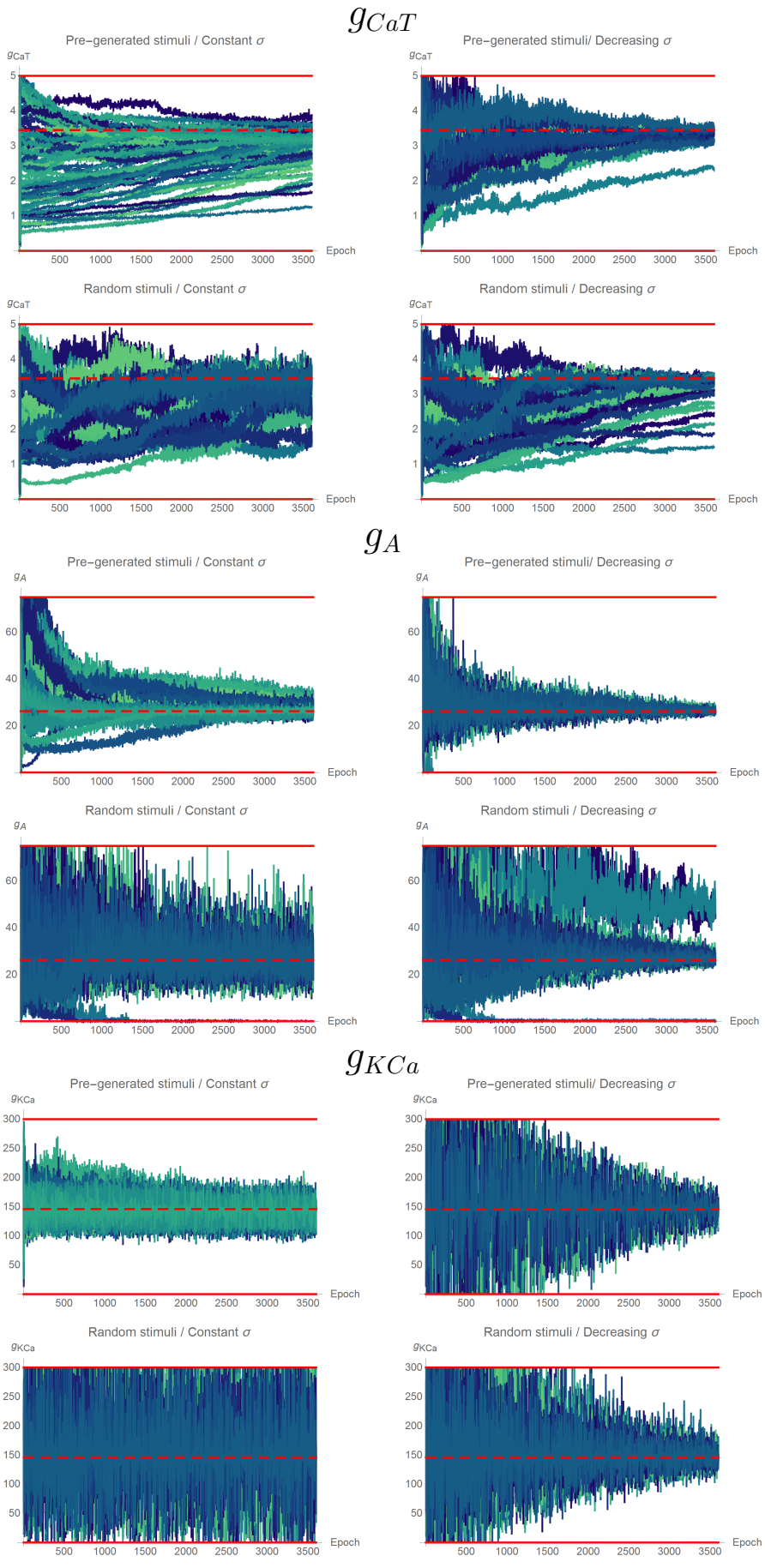
g_{CaT}
Pre−generated stimuli / Constant σ
Pre−generated stimuli/ Decreasing σ
Random stimuli / Constant σ
Random stimuli / Decreasing σ
g_{CaT}
g_A
Pre−generated stimuli / Constant σ
Pre−generated stimuli/ Decreasing σ
Random stimuli / Constant σ
Random stimuli / Decreasing σ
g_A
g_{KCa}
Pre−generated stimuli / Constant σ
Pre−generated stimuli/ Decreasing σ
Random stimuli / Constant σ
Random stimuli / Decreasing σ
g_{KCa}
Epoch
500 1000 1500 2000 2500 3000 3500

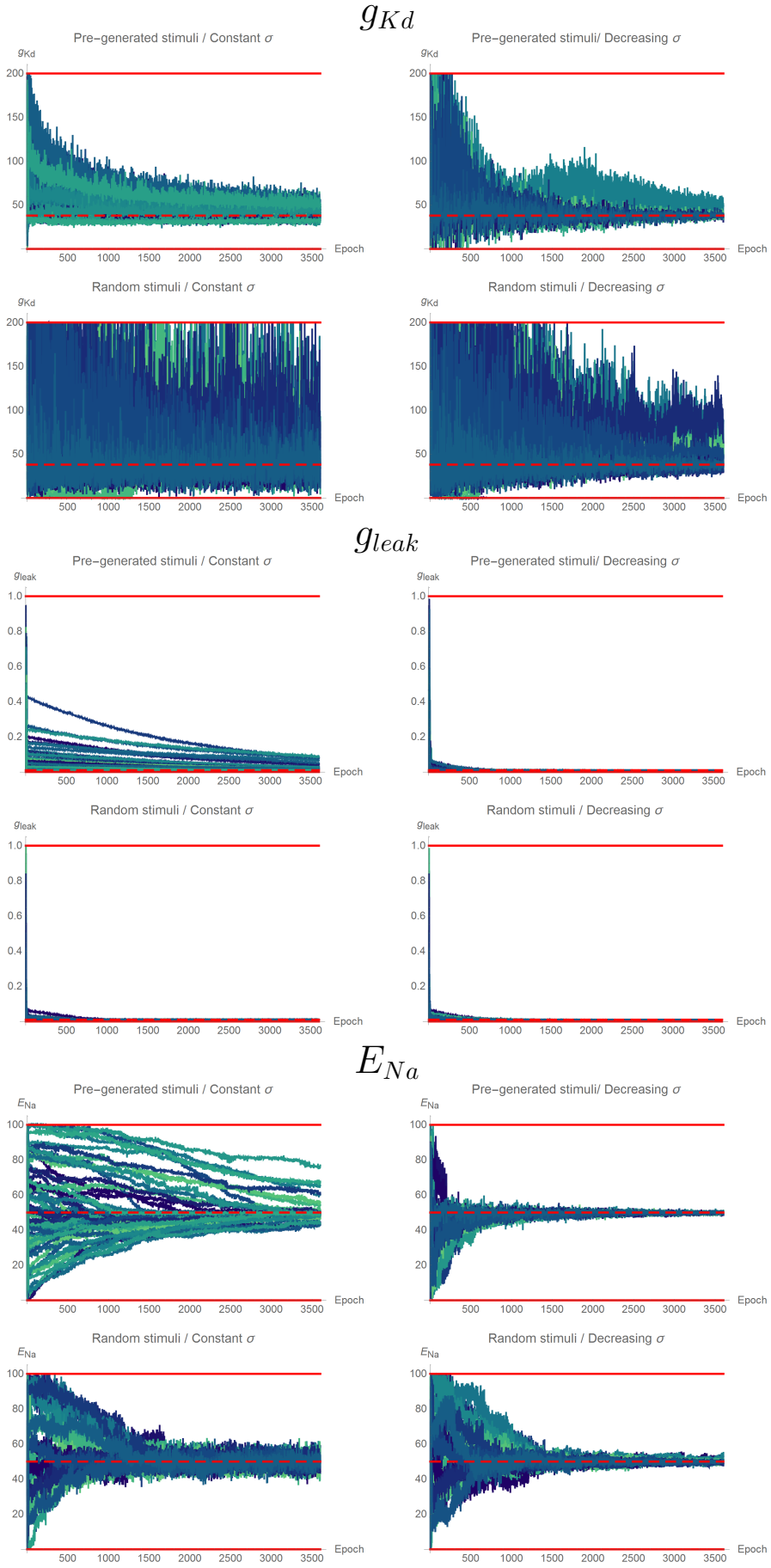
g_{Kd}
Pre−generated stimuli / Constant σ
Pre−generated stimuli/ Decreasing σ
Random stimuli / Constant σ
Random stimuli / Decreasing σ
g_{leak}
Pre−generated stimuli / Constant σ
Pre−generated stimuli/ Decreasing σ
Random stimuli / Constant σ
Random stimuli / Decreasing σ
E_{Na}
Pre−generated stimuli / Constant σ
Pre−generated stimuli/ Decreasing σ
Random stimuli / Constant σ
Random stimuli / Decreasing σ
Epoch

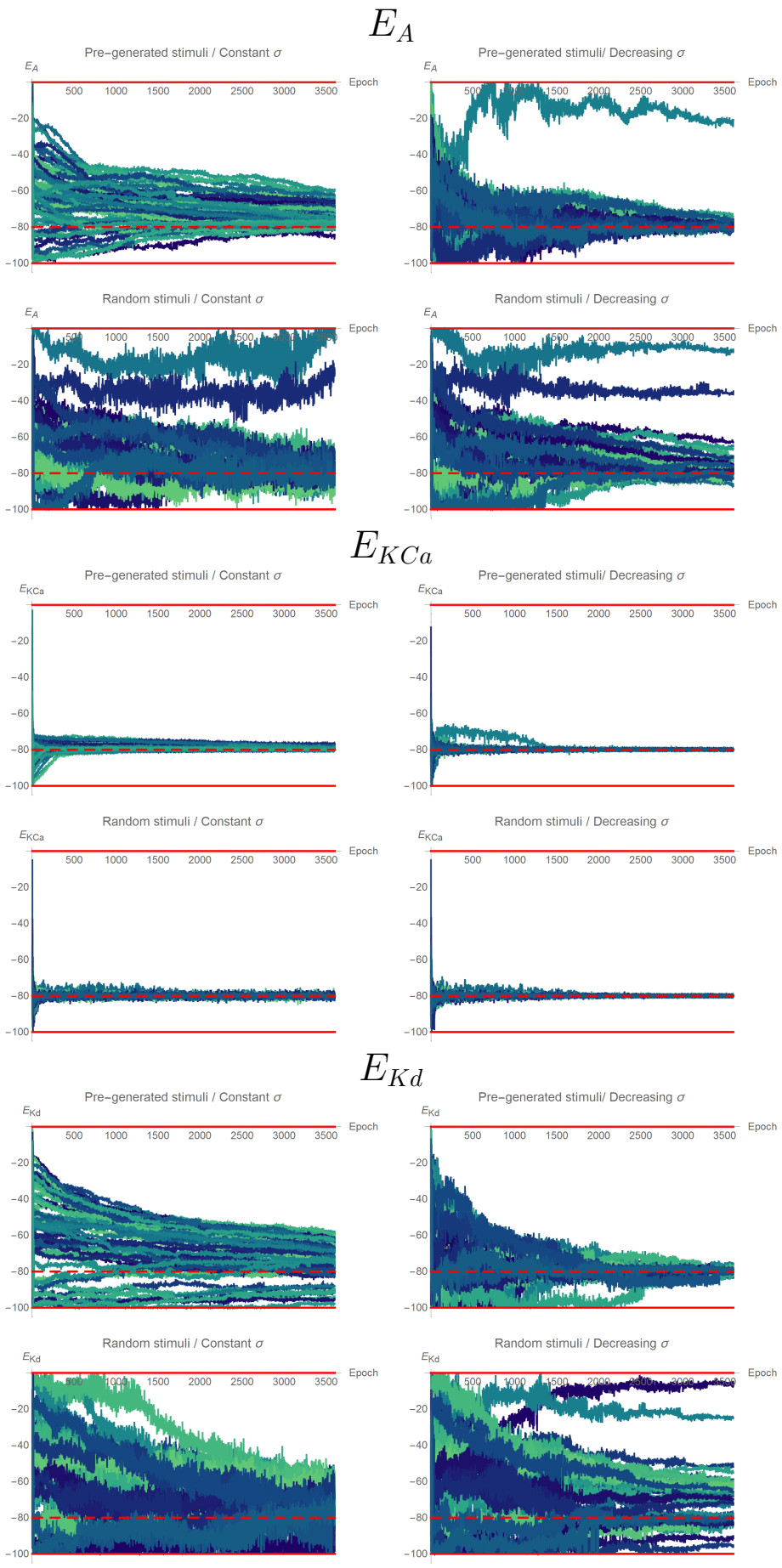
E_A
Pre−generated stimuli / Constant σ
Pre−generated stimuli/ Decreasing σ
Random stimuli / Constant σ
Random stimuli / Decreasing σ
E_{KCa}
Pre−generated stimuli / Constant σ
Pre−generated stimuli/ Decreasing σ
Random stimuli / Constant σ
Random stimuli / Decreasing σ
E_{Kd}
Pre−generated stimuli / Constant σ
Pre−generated stimuli/ Decreasing σ
Random stimuli / Constant σ
Random stimuli / Decreasing σ
Epoch
500 1000 1500 2000 2500 3000 3500
−20 −40 −60 −80 −100

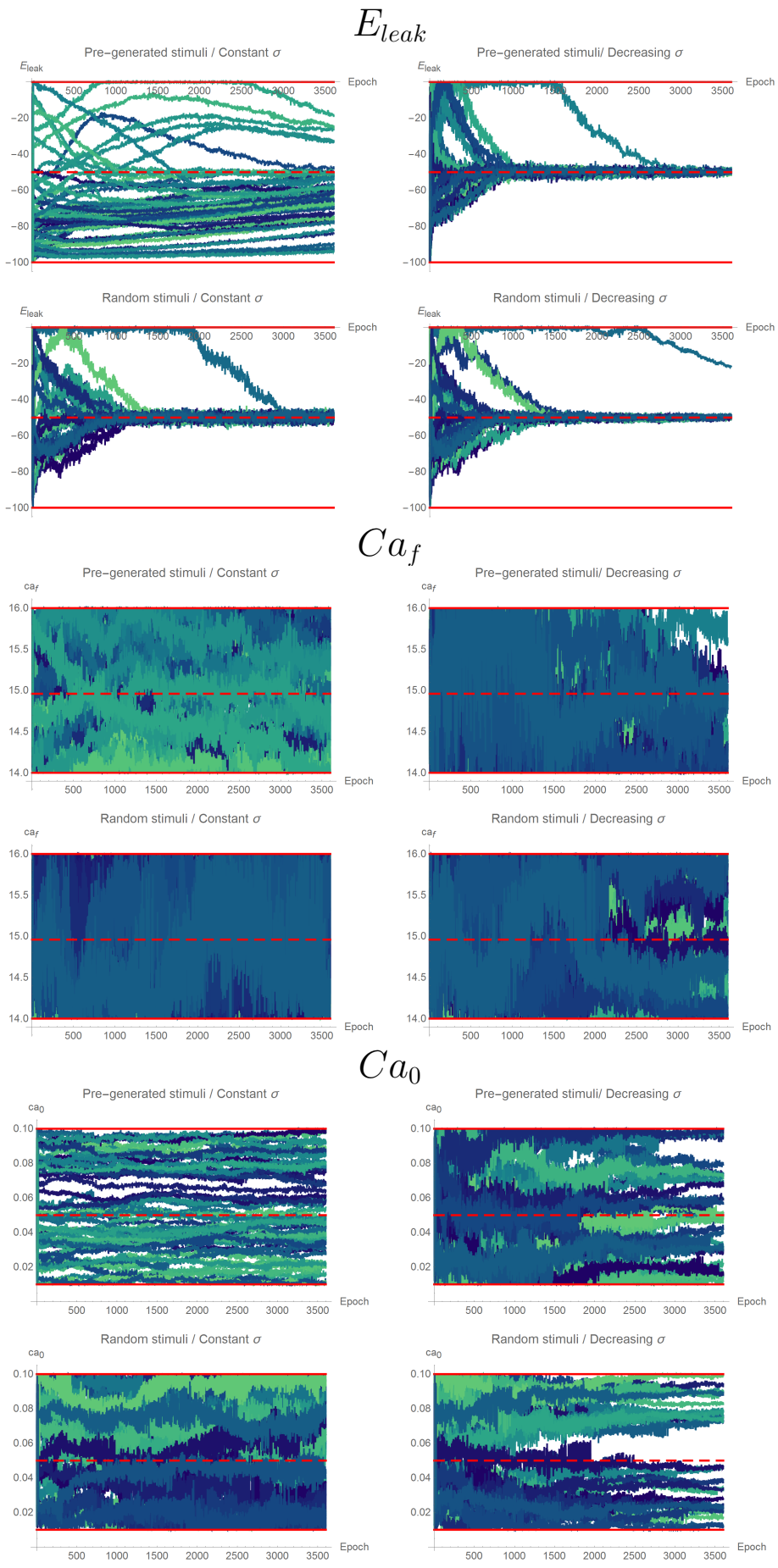
E_{leak}
Pre−generated stimuli / Constant σ
Pre−generated stimuli/ Decreasing σ
Random stimuli / Constant σ
Random stimuli / Decreasing σ
E_{leak}
Epoch
Ca_f
ca_f
Ca_0
ca_0

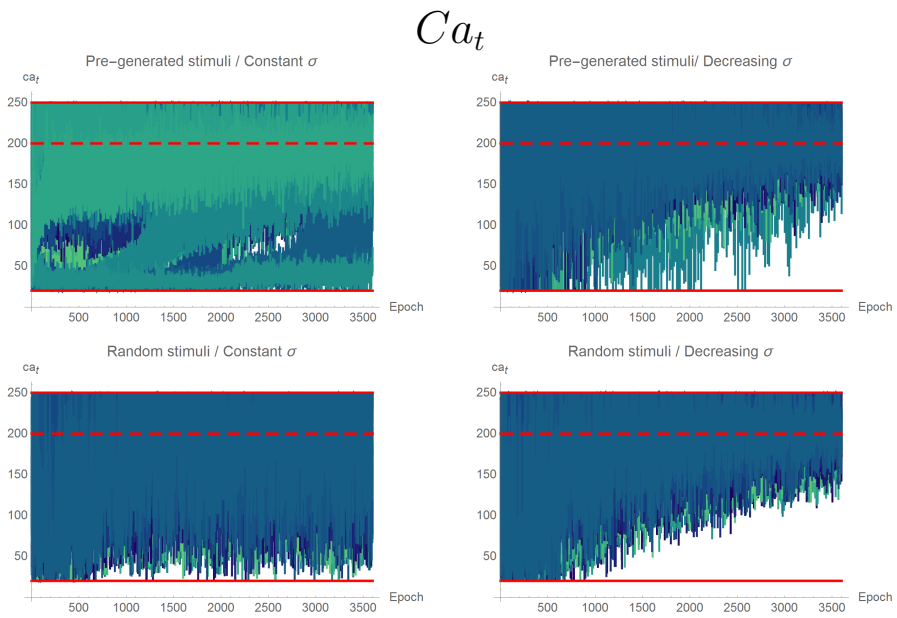
Ca_t
Pre−generated stimuli / Constant σ
Pre−generated stimuli/ Decreasing σ
Random stimuli / Constant σ
Random stimuli / Decreasing σ
ca_t
250
200
150
100
50
500
1000
1500
2000
2500
3000
3500
Epoch

Bibliography

[1] J. Golowasch, M. S. Goldman, L. Abbott, and E. Marder, "Failure of averaging in the construction of a conductance-based neuron model", *Journal of Neurophysiology*, vol. 87, no. 2, pp. 1129–1131, 2002.

[2] A. L. Hodgkin and A. F. Huxley, "A quantitative description of membrane current and its application to conduction and excitation in nerve", *The Journal of physiology*, vol. 117, no. 4, p. 500, 1952.

[3] Z. Liu, J. Golowasch, E. Marder, and L. Abbott, "A model neuron with activity-dependent conductances regulated by multiple calcium sensors", *The Journal of neuroscience*, vol. 18, no. 7, pp. 2309–2320, 1998.

[4] A. L. Hodgkin and B. Katz, "The effect of sodium ions on the electrical activity of the giant axon of the squid", *The Journal of physiology*, vol. 108, no. 1, p. 37, 1949.

[5] A. L. Hodgkin, "The ionic basis of electrical activity in nerve and muscle", *Biological Reviews*, vol. 26, no. 4, pp. 339–409, 1951.

[6] D. Aidley, *The Physiology of Excitable Cells*. Cambridge University Press, 1998, ISBN: 9780521574211.

[7] T. Narahashi, T. Deguchi, N. Urakawa, and Y. Ohkubo, "Stabilization and rectification of muscle fiber membrane by tetrodotoxin", *American Journal of Physiology – Legacy Content*, vol. 198, no. 5, pp. 934–938, 1960, ISSN: 0002-9513.

[8] T. Narahashi, J. W. Moore, and W. R. Scott, "Tetrodotoxin blockage of sodium conductance increase in lobster giant axons", *The Journal of general physiology*, vol. 47, no. 5, pp. 965–974, 1964.

[9] Y. Nakamura, S. Nakajima, and H. Grundfest, "The action of tetrodotoxin on electrogenic components of squid giant axons", *The Journal of general physiology*, vol. 48, no. 6, pp. 985–996, 1965.

[10] M Takata, J. Moore, C. Kao, and F. Fuhrman, "Blockage of sodium conductance increase in lobster giant axon by tarichatoxin (tetrodotoxin)", *The Journal of general physiology*, vol. 49, no. 5, pp. 977–988, 1966.

[11] B. Hille, "The selective inhibition of delayed potassium currents in nerve by tetraethylammonium ion", *The Journal of general physiology*, vol. 50, no. 5, pp. 1287–1302, 1967.

[12] K. Graubard and D. K. Hartline, "Voltage clamp analysis of intact stomatogastric neurons", *Brain research*, vol. 557, no. 1-2, pp. 241–254, 1991.

[13] C. Miller, E. Moczydlowski, R. Latorre, and M. Phillips, "Charybdotoxin, a protein inhibitor of single ca2+-activated k+ channels from mammalian skeletal muscle", *Nature*, vol. 313, no. 6000, pp. 316–318, 1985.

[14] J. Golowasch and E Marder, "Ionic currents of the lateral pyloric neuron of the stomatogastric ganglion of the crab", *Journal of Neurophysiology*, vol. 67, no. 2, pp. 318–331, 1992.

[15] M. C. Jost, D. M. Hillis, Y. Lu, J. W. Kyle, H. A. Fozzard, and H. H. Zakon, "Toxin-resistant sodium channels: Parallel adaptive evolution across a complete gene family", *Molecular biology and evolution*, vol. 25, no. 6, pp. 1016–1024, 2008.

[16] L. K. Kaczmarek and I. B. Levitan, *Neuromodulation: The biochemical control of neuronal excitability*. Oxford University Press, USA, 1987.

[17] G. Turrigiano, G. LeMasson, and E. Marder, "Selective regulation of current densities underlies spontaneous changes in the activity of cultured neurons", *The Journal of neuroscience*, vol. 15, no. 5, pp. 3640–3652, 1995.

[18] D. K. Hartline and D. M. Maynard, "Motor patterns in the stomatogastric ganglion of the lobster panulirus argus", *Journal of Experimental Biology*, vol. 62, no. 2, pp. 405–420, 1975.

[19] R. M. Harris-Warrick and R. E. Flamm, "Multiple mechanisms of bursting in a conditional bursting neuron", *The Journal of neuroscience*, vol. 7, no. 7, pp. 2113–2128, 1987.

[20] A. Taddese and B. P. Bean, "Subthreshold sodium current from rapidly inactivating sodium channels drives spontaneous firing of tuberomammillary neurons", *Neuron*, vol. 33, no. 4, pp. 587–600, 2002.

[21] O. Kiehn and R. M. Harris-Warrick, "5-ht modulation of hyperpolarization-activated inward current and calcium-dependent outward current in a crustacean motor neuron", *Journal of Neurophysiology*, vol. 68, no. 2, pp. 496–508, 1992.

[22] A. Tierney and R. Harris-Warrick, "Physiological role of the transient potassium current in the pyloric circuit of the lobster stomatogastric ganglion", *Journal of neurophysiology*, vol. 67, no. 3, pp. 599–609, 1992.

[23] B. Zhang, J. F. Wootton, and R. M. Harris-Warrick, "Calcium-dependent plateau potentials in a crab stomatogastric ganglion motor neuron. ii. calcium-activated slow inward current", *Journal of Neurophysiology*, vol. 74, no. 5, pp. 1938–1946, 1995.

[24] D. K. Hartline, D. F. Russell, J. A. Raper, and K. Graubard, "Special cellular and synaptic mechanisms in motor pattern generation", *Comparative Biochemistry and Physiology Part C: Comparative Pharmacology*, vol. 91, no. 1, pp. 115–131, 1988.

[25] D. K. Hartline and D. V. Gassie, "Pattern generation in the lobster (panulirus) stomatogastric ganglion", *Biological Cybernetics*, vol. 33, no. 4, pp. 209–222, ISSN: 1432-0770. DOI: 10.1007/BF00337410.

[26] D. K. Hartline and K. Graubard, "Cellular and synaptic properties in the crustacean stomatogastric nervous system", *Dynamic Biological Networks: The Stomatogastric Nervous System*, pp. 31–85, 1992.

[27] M. Gurkiewicz and A. Korngreen, "A numerical approach to ion channel modelling using whole-cell voltage-clamp recordings and a genetic algorithm", *PLoS Comput Biol*, vol. 3, no. 8, e169, 2007.

[28] L. Buhry, S. Saïghi, A. Giremus, E. Grivel, and S. Renaud, "Parameter estimation of the hodgkin-huxley model using metaheuristics: Application to neuromimetic analog integrated circuits", in *Biomedical Circuits and Systems Conference, 2008. BioCAS 2008. IEEE*, IEEE, 2008, pp. 173–176.

[29] N. Keren, N. Peled, and A. Korngreen, "Constraining compartmental models using multiple voltage recordings and genetic algorithms", *Journal of neurophysiology*, vol. 94, no. 6, pp. 3730–3742, 2005.

[30] C. Rossant, D. F. Goodman, J. Platkiewicz, and R. Brette, "Automatic fitting of spiking neuron models to electrophysiological recordings", *Frontiers in neuroinformatics*, vol. 4, p. 2, 2010.

[31] G. Seemann, S Lurz, D. Keller, D. Weiss, E. Scholz, and O Dössel, "Adaption of mathematical ion channel models to measured data using the particle swarm optimization", in *4th European Conference of the International Federation for Medical and Biological Engineering*, Springer, 2009, pp. 2507–2510.

[32] A. R. Willms, "Neurofit: Software for fitting hodgkin–huxley models to voltage-clamp data", *Journal of neuroscience methods*, vol. 121, no. 2, pp. 139–150, 2002.

[33] J. C. Quinn and H. D. Abarbanel, "Data assimilation using a gpu accelerated path integral monte carlo approach", *Journal of Computational Physics*, vol. 230, no. 22, pp. 8168–8178, 2011.

[34] R. Ben-Shalom, A. Aviv, B. Razon, and A. Korngreen, "Optimizing ion channel models using a parallel genetic algorithm on graphical processors", *Journal of neuroscience methods*, vol. 206, no. 2, pp. 183–194, 2012.

[35] T. Blickle and L. Thiele, *A comparison of selection schemes used in genetic algorithms*, 1995.

[36] T. Nowotny, "Closed-loop computational electrophysiolgy", Unpublished seminar presentation, 2015.

[37] C. French, P Sah, K. Buckett, and P. Gage, "A voltage-dependent persistent sodium current in mammalian hippocampal neurons.", *The Journal of General Physiology*, vol. 95, no. 6, pp. 1139–1157, 1990.